

# We are IntechOpen, the world's leading publisher of Open Access books Built by scientists, for scientists

4,800

Open access books available

122,000

International authors and editors

135M

Downloads

Our authors are among the

154

Countries delivered to

TOP 1%

most cited scientists

12.2%

Contributors from top 500 universities



WEB OF SCIENCE™

Selection of our books indexed in the Book Citation Index  
in Web of Science™ Core Collection (BKCI)

Interested in publishing with us?  
Contact [book.department@intechopen.com](mailto:book.department@intechopen.com)

Numbers displayed above are based on latest data collected.  
For more information visit [www.intechopen.com](http://www.intechopen.com)



# Tellurite Glass and Its Application in Lasers

*Pengfei Wang, Shijie Jia, Xiaosong Lu, Yuxuan Jiang, Jibo Yu, Xin Wang, Shunbin Wang and Elfed Lewis*

## Abstract

This chapter provides expert coverage of the physical properties of new noncrystalline solids—tellurite glass and the latest laser applications of the material—offering insights into innovative applications for laser and sensing devices, among others. In particular, there is a focus on specialty optical fibers, supercontinuum generation and laser devices, and luminescence properties for laser applications. This chapter also addresses the fabrication and optical properties and uses of tellurite glasses in optical fibers and optical microcavities, the significance of from near infrared (NIR) to mid-infrared (MIR) emissions and the development of tellurite glass-based microcavity lasers. The important attributes of these tellurite glasses and their applications in lasers were discussed in this chapter.

**Keywords:** tellurite glass, fiber lasers, supercontinuum sources, specialty fibers, microcavity lasers

## 1. Introduction of tellurite glass

Tellurite glasses are noncrystalline solids with many applications in photonics, appear in a wide range of compositions, and can be operated over a large temperature range [1–4]. Tellurite glasses have been studied for more than 150 years [5], but more recent versions have been produced with purities exceeding 98.5% [6]. They are characterized by a low melting point and the absence of hygroscopic properties, and hence tellurite glasses have limited the application of phosphate and borate glasses and aroused widespread interest in the field of photonics and associated technologies. Moreover, they have high density and a low transition temperature [7, 8]. Their optical properties include relatively high refractive index, high nonlinear refractive index, high dielectric constant, as well as good chemical stability and a wide infrared (IR) transmission range (1–6  $\mu\text{m}$ ) [9–11].

In 1952, Stanworth [1] conducted preliminary research on the formation and structure of tellurite glass. The main raw material is  $\text{TeO}_2$  and at that time this was relatively expensive, and hence tellurite glass was considered to be of low practical value and had not been further studied. Since the late 1980s to the mid of 1990s [12, 13], considerable progress had been made in the advancement and understanding of the optical and physical properties of new tellurite glasses, including their molecular structure and bonding properties.

Research in tellurite glass-based broadband fiber amplifiers was initially concentrated around erbium-doped tellurite fibers. This was primarily due to its

relatively broadband gain spectrum, which led to it attracting a great deal of research attention which has persisted up to the present. Currently, many world-class university-based research institutions and industrial companies have investigated the potential of tellurite glass for use in fibers, and this has resulted in rapid progress. In this section, the composition, structure, and thermal stability of tellurite glasses will be considered.

### 1.1 Composition of tellurite glass

The selection of tellurite glass components when used in binary combinations with other materials is very important. It directly affects the glass-forming ability, thermal stability, refractive index, rare earth ion doping concentration, and spectral characteristics. **Table 1** lists the range of TeO<sub>2</sub> glass formation in several binary tellurite glass systems. **Table 1** shows that TeO<sub>2</sub> exhibits the largest glass formation range in the case of the three binary systems TeO<sub>2</sub>-ZnO (100–52 mol%), TeO<sub>2</sub>-WO<sub>3</sub> (94.7–61.3 mol%), and TeO<sub>2</sub>-TiO<sub>2</sub> (100–52 mol%).

The structure of tellurite glass is always generally based on binary systems. The ternary and multivariate tellurite glass systems have been generally used as rare earth-doped substrates for the investigation of the waveguide spectral properties. The diversity of components has helped to improve the chemical and thermal stability of tellurite glass-based devices. **Table 2** [14] includes the composition of the tellurite glass systems that have been reported in recent years. In all cases TeO<sub>2</sub> was used as the glass-forming material, and its content was generally higher than 50 mol% (as shown in **Table 1**). Other oxides were generally used as modified bodies. From **Table 2** [14], it can be seen that the research objects of the binary system were more diversified. In addition to the common monovalent alkali metal oxides and divalent alkaline earth metal oxides, many other oxide components were involved, including CeO<sub>2</sub>, SmO<sub>2</sub>, V<sub>2</sub>O<sub>5</sub>, etc. It should be pointed out that in the case of the ternary tellurite glass systems, the TeO<sub>2</sub>-ZnO-R<sub>m</sub>O<sub>n</sub> and TeO<sub>2</sub>-WO<sub>3</sub>-R<sub>m</sub>O<sub>n</sub> glass systems were the most widely investigated, because these two systems possessed a wide range of glass formation regions and a wide range of adjustable components.

### 1.2 The structure of tellurite glasses

Early research was reported to suggest that the molecular structure of pure tellurite glass molecules comprised TeO<sub>4</sub> double triangular bipyramids (tbp's) [36].

Composition	Glass formation range TeO <sub>2</sub> mol%	Composition	Glass formation range TeO <sub>2</sub> mol%
Cs <sub>2</sub> O	98.0–87.5	ZnO	100–52.5
Rb <sub>2</sub> O	96.5–73.0	CdO	60.0–48.0
K <sub>2</sub> O	95.5–77.0	PbO	60.0–48.0
Na <sub>2</sub> O	91.5–59.5	Bi <sub>2</sub> O <sub>3</sub>	66–60
Li <sub>2</sub> O	87.0–69.5	WO <sub>3</sub>	94.7–61.3
BaO	93.0–80.0	Nb <sub>2</sub> O <sub>5</sub>	100–73.2
TiO <sub>2</sub>	100–52.5		

**Table 1.**  
*The formation range of binary system tellurite glass.*

Binary system	Ternary system	Multicomponent glass system
TeO <sub>2</sub> -R <sub>2</sub> O (R = Li, Na, K, Rb, Cs, Ti) [15]	TeO <sub>2</sub> -ZnO-R <sub>2</sub> O (R = Li, Na, K) [16]	TeO <sub>2</sub> -ZnO-B <sub>2</sub> O <sub>3</sub> -K <sub>2</sub> O [10]
TeO <sub>2</sub> -MO (M = Zn [17], Ba, Pb) [18]	TeO <sub>2</sub> -ZnO-RO (R = Ba, Mg, Sr) [19]	TeO <sub>2</sub> -ZnO-GeO <sub>2</sub> -Na <sub>2</sub> O [20]
TeO <sub>2</sub> -M <sub>3</sub> O <sub>4</sub> (M = Co) [21]	TeO <sub>2</sub> -WO <sub>3</sub> -R <sub>2</sub> O (R = Li, Na, K) [22]	TeO <sub>2</sub> -ZnO-B <sub>2</sub> O <sub>3</sub> -GeO <sub>2</sub> -Na <sub>2</sub> O [23]
TeO <sub>2</sub> -M <sub>2</sub> O <sub>3</sub> (M = Sm, La) [21]	TeO <sub>2</sub> -WO <sub>3</sub> -BaO [15]	TeO <sub>2</sub> -ZnO-Na <sub>2</sub> O-Bi <sub>2</sub> O <sub>3</sub> [24]
TeO <sub>2</sub> -CeO <sub>2</sub> [21]	TeO <sub>2</sub> -WO <sub>3</sub> -Bi <sub>2</sub> O <sub>3</sub> [15]	TeO <sub>2</sub> -ZnO-WO <sub>3</sub> -TiO <sub>2</sub> -Na <sub>2</sub> O [25]
TeO <sub>2</sub> -M <sub>2</sub> O <sub>5</sub> (M = P [21], V [26], Nb [27])	TeO <sub>2</sub> -WO <sub>3</sub> -Nb <sub>2</sub> O <sub>5</sub> [28]	TeO <sub>2</sub> -ZnO-Nb <sub>2</sub> O <sub>5</sub> -Nb <sub>2</sub> O <sub>3</sub> [29]
TeO <sub>2</sub> -MO <sub>3</sub> (M = W [30], Mo [31])	TeO <sub>2</sub> -B <sub>2</sub> O <sub>3</sub> -M <sub>2</sub> O <sub>3</sub> (M = Al, Ga, Sc, La, Bi) [16]	TeO <sub>2</sub> -Li <sub>2</sub> O-Nb <sub>2</sub> O <sub>5</sub> -K <sub>2</sub> O [32]
TeO <sub>2</sub> -PbF <sub>2</sub> [33]	TeO <sub>2</sub> -K <sub>2</sub> O-La <sub>2</sub> O <sub>3</sub> [34]	TeO <sub>2</sub> -ZnO-Nb <sub>2</sub> O <sub>5</sub> -Gd <sub>2</sub> O <sub>3</sub> [35]

**Table 2.**  
 Tellurite glass systems [14].

In this polyhedron, one Te atom is surrounded by four oxygen atoms, of which two oxygen atoms O<sub>eq</sub> are at the equator position and the other two oxygen atoms O<sub>ax</sub> at the axial position. The Te atoms are linked by O<sub>ax</sub> or O<sub>eq</sub> into Te—O—Te; an apex of the tetrahedron on the equatorial plane remains unoccupied by oxygen atoms and is occupied by Te's lone electron pair [16]. This special polyhedral structure and the chemical bonding were different from the traditional glass-forming bodies (B<sub>2</sub>O<sub>3</sub>, SiO<sub>2</sub>, GeO<sub>2</sub>, and P<sub>2</sub>O<sub>5</sub>), which determined the specificity of the tellurite glass structure.

Some scholars used various testing methods to conduct research and analysis on tellurite glasses, especially binary system tellurite glass. Jha et al. [37] considered that the main structural units of tellurite glass were TeO<sub>4</sub> double triangular bipyramids (tbp's) and TeO<sub>3</sub> bipyramids (bp's) triangular pyramids. In 1995, Neov et al. [36] were the first to perform neutron diffraction analysis on lithium tellurite glass and pointed out that in addition to the TeO<sub>4</sub> structural unit, a deformed double triangular pyramid TeO<sub>3+1</sub> existed in the glass network. One of the Te—O bonds was significantly longer than the other three. Due to the short-range similarity between the glass and crystal structures, the structure of tellurite glasses can be studied and analyzed based on the structure of tellurite crystals with the same composition. Sakida et al. [32] compared the Raman spectra of alkali tellurite crystals, pure tellurite glasses, and alkali tellurite glasses. The resulting Raman spectra were considered to correspond to structural elements in the glass. TeO<sub>4</sub> (tbp's) double triangular bipyramids were finally transformed into a TeO<sub>3</sub> (bp's) triangular pyramid by TeO<sub>3+1</sub>. Tatsumisago et al. [38] studied the change of tellurite glass structure with temperature using Raman spectroscopy. Throughout the above research, the general laws could be classified as follows:

1. It was generally considered that there were two kinds of structural units that form a tellurite glass network. One was TeO<sub>4</sub> (tbp's) double triangular pyramid in which the Te atoms were arranged as a four ligand, and the other

was  $\text{TeO}_3$  (bp's) triangular pyramid in which the Te atoms were in a triple coordination. It was considered that there were generally five kinds of structural units in alkali tellurite crystals, as shown in **Figure 1(a-e)**.  $Q_m^n$  can be used to represent the structural unit in **Figure 1**, where n is the number of bridge oxygen molecules in the  $[\text{TeO}_4]$  group and m represents the number of covalent bonds. Research on the distribution of various structural units (a-e) in tellurite glass has become a significant focus of research in this field.

- When an alkali metal oxide or alkaline earth metal oxide was introduced into tellurite glass as a network modifier, the original glass network structure was destroyed.  $\text{TeO}_4$  (tbp's) double triangular pyramid was finally transformed into  $\text{TeO}_3$  (bp's) triangular pyramid by  $\text{TeO}_{3+1}$ . Sekiya [39] investigated the  $\text{TeO}_2\text{-MO}_{1/2}$  binary system and considered that when the alkali metal oxide content was low, the glass was composed of  $\text{TeO}_4$  (tbp's) double triangular pyramid and  $\text{TeO}_{3+1}$  polyhedron. When the alkali content was less than 20 mol %, the number of  $\text{TeO}_{3+1}$  polyhedra increased with the increase of the alkali metal oxide content. When the alkali content was between 20 and 30 mol%,  $\text{TeO}_3$  (bp's) triangular pyramids with non-bridged oxygen bonds appeared in the glass network structure, and the numbers of  $\text{TeO}_4$  (tbp's) and  $\text{TeO}_{3+1}$  decreased accordingly. When the alkali metal oxide content exceeded 30 mol %, the  $\text{Te}_2\text{O}_5^{2-}$  polyhedron was formed in the network structure. When the alkali metal oxide content was greater than 50 mol%, it was considered that the glass network structure at this time was composed of  $\text{TeO}_3$  (bp's) polyhedrons,  $\text{TeO}_{3+1}$  polyhedrons, and independent  $\text{Te}_2\text{O}_5^{2-}$  and  $\text{TeO}_3^{2-}$ . At this time, the number of  $\text{TeO}_4$  in the glass was very small, and the glass structure had become extremely complex.
- Temperature also affects the structure of tellurite glass. For example, when the glass temperature was gradually increased and exceeded the melting temperature, the  $\text{TeO}_4$  (tbp's) double triangular pyramid would also be transformed into a  $\text{TeO}_3$  (bp's) triangular pyramid. This is mainly due to the fact that  $\text{Te-O}_{ax}$  is caused by fracture with increasing temperature, and its structural transformation process is shown in **Figure 2**.

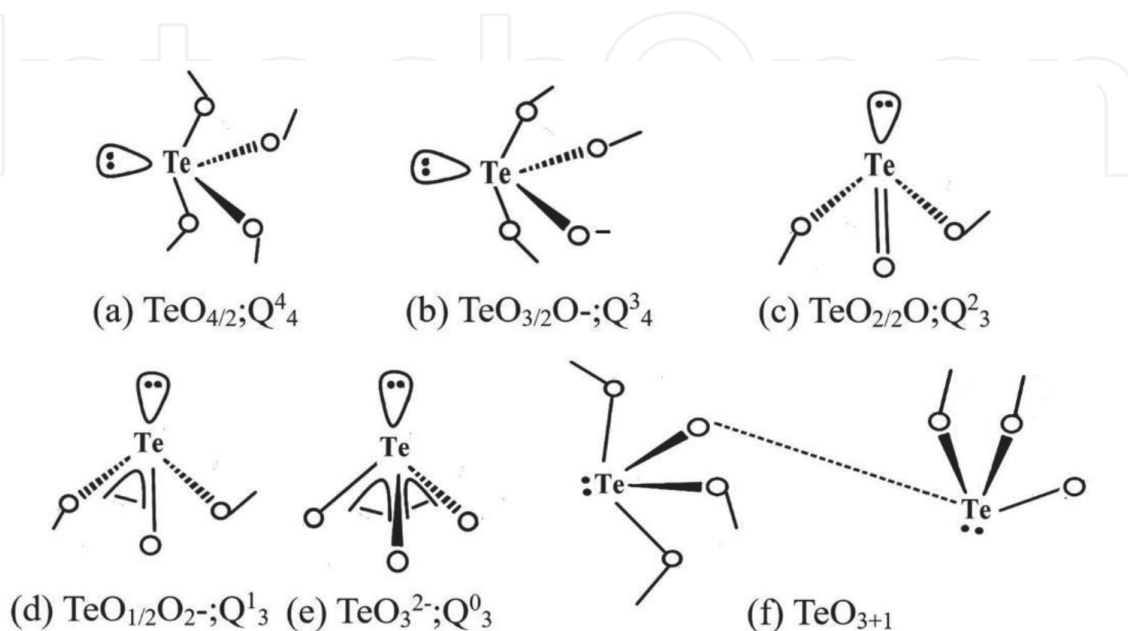


**Figure 1.**

(a-e) Five basic structural units in alkali tellurite crystals. (f) Deformed bitriangular cone  $\text{TeO}_{3+1}$ .



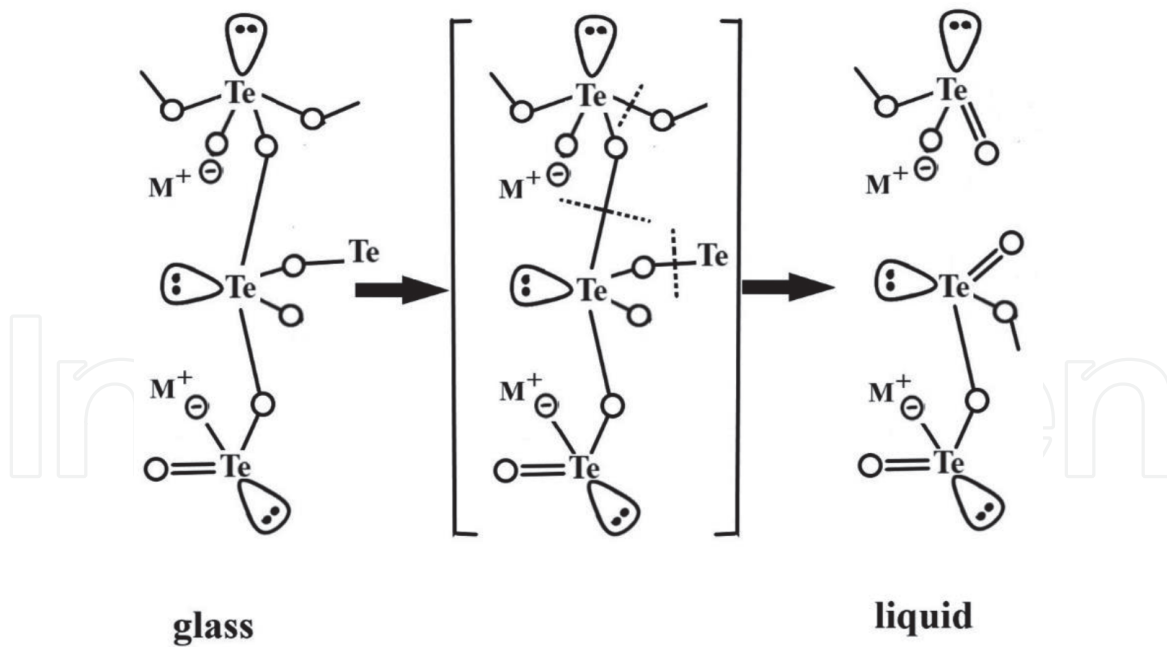


**Figure 2.**  
 Transformation of glass structure during heating.

### 1.3 Thermal properties of tellurite glass

The thermal stability of tellurite glass is primarily dictated by composition and the doping concentration of rare earth ions. The characteristic glass temperature values include glass transition temperature  $T_g$ , incipient crystallization temperature  $T_x$ , peak crystallization temperature  $T_c$ , and glass-melting temperature  $T_m$ .

The thermal stability of glass is usually expressed by  $\Delta T$ , which is the differential value between  $T_x$  and  $T_g$ . A higher value of  $\Delta T$  generally means that the glass has good thermal stability. If the value of the  $T_x$  is close to  $T_f$ , it will lead to crystallization during a fiber drawing process which leads to an increase in the loss (attenuation) of the resulting glass fiber. **Table 3** includes a listing of several kinds of tellurite glass with good thermal stability together with their characterized glass temperatures ( $T_g$ ,  $T_x$ , and  $\Delta T$ ). In the case of  $\text{TeO}_2\text{-R}_2\text{O}$  ( $R = \text{Li, Na, K, or other alkali metal}$ ) tellurite glass systems, as the content of the alkali metal oxide increases,  $T_g$  gradually increases, while  $T_x$  remains almost unchanged. Consequently, the  $\Delta T$  increases correspondingly, and the resistance against crystallization of the tellurite glass also increases.

In addition, the introduction of rare earth ions also has an influence on the thermal stability of tellurite glasses. For example, 1 wt%  $\text{Pr}_2\text{O}_3$  introduced to a

Glass component	$T_g$ (°C)	$T_x$ (°C)	$T_x - T_g$ (°C)
85TeO <sub>2</sub> -15Na <sub>2</sub> O	277	447	170
70TeO <sub>2</sub> -10ZnO-20Li <sub>2</sub> O	265	392	127
70TeO <sub>2</sub> -20ZnO-10BaO [40]	339	495	156
82.5TeO <sub>2</sub> -7.5WO <sub>3</sub> -10Nb <sub>2</sub> O <sub>5</sub> [41]	391	562	171
80TeO <sub>2</sub> -10WO <sub>3</sub> -10Nb <sub>2</sub> O <sub>5</sub> -1Yb <sub>2</sub> O <sub>3</sub> [42]	404	566	162
60TeO <sub>2</sub> -20ZnO-7.5B <sub>2</sub> O <sub>3</sub> -7.5GeO <sub>2</sub> -5K <sub>2</sub> O	200 ± 5	378 ± 2	178

**Table 3.**  
 Characteristic temperature of tellurite glasses.

75TeO<sub>2</sub>-20ZnO-5Na<sub>2</sub>O [43] system increases the  $\Delta T$  value from 118 to 150°C, while 1 wt% Er<sub>2</sub>O<sub>3</sub> introduced to 90TeO<sub>2</sub>-10P<sub>2</sub>O<sub>5</sub> [44] system decreases the  $\Delta T$  value from 147 to 101°C. Furthermore, the concentration of the rare earth ion has a significant influences on the  $\Delta T$  value of the 75TeO<sub>2</sub>-20ZnO-5Na<sub>2</sub>O [45] glass system.

## **2. Fiber lasers and fiber amplifier based on tellurite glass fibers**

### **2.1 Tellurite glass-based fiber lasers**

Since the discovery of the first ruby laser (Maiman in 1960), the laser has attracted worldwide attention for its excellent collimation, high brightness, and monochromaticity [46]. Since then, the development of the laser has accelerated. In 1961, Javan et al. developed the helium-neon gas laser [47], and in 1962, Hall et al. created the GaAs coherent light emission [48]. In 1963, Koester et al. first proposed the idea of fiber lasers and amplifiers [49]. However, due to the shortcomings of the optical fiber at that time, the development of the optical fiber laser was slow during this period. In 1966, Gao et al. proposed the basic concept of optical fiber communication [50]. Subsequently, optical fiber communication underwent a major research and development stage (1966–1976), a practical application stage (1976–1986), and a large-scale optical fiber communication infrastructure construction stage after 1986. With the rapid development of optical communication, optical fiber manufacturing technology and semiconductor laser production technology have matured, which formed the foundation for the subsequent development of doped fibers, optical fiber lasers, and fiber amplifiers.

The tellurite fiber laser is based on a tellurite glass fiber which acts as a gain medium. The first significant characterization of the optical properties of tellurite glass in fiber form was reported in 1994 [12]. In 1997, Mori et al. realized that Er<sup>3+</sup>-doped tellurite glass fiber could be used for broadband optical amplifiers [13]. Further research on tellurite fiber was initiated worldwide driven by the development of the communication industry. Over the next few years, Japan's NTT led the research in this field. They fabricated tellurite fiber with a loss of 0.02 dB/m and developed the first erbium-doped tellurite fiber amplifier (EDTFA) module for use in commercial WDM systems [51]. Further subsequent significant contributions to tellurite fiber laser development have been used by several university groups as well as industry-based research institutions including American Corning corporation, Fujitsu and Nippon of Japan, Korea's ETRI, etc.

Tellurite glass has a broad transmission window in the infrared wavelength range which extends up to 6  $\mu\text{m}$ , a relatively low phonon energy of about 700  $\text{cm}^{-1}$ , and high solubility of rare earth ions. It is therefore an excellent host material for constructing single and high repetition frequency fiber lasers. Yao et al. measured the transmission spectrum of 2-mm-thick glass samples after they were immersed in deionized water for 12 days [52], and the results are shown in **Figure 3**. There was no obvious change in the transmission spectra, and no hydrated layer was formed at the end face of the tellurite glass, which proves its great resistance to water. Several researchers have studied the reduction of water molecules and hydroxyl groups, in order to further improve the performance of tellurite glass materials used in mid-infrared fiber lasers. Specific test procedures included melting the glass in a dry atmosphere, raw material dehydration, and the use of fluoride [52] or chloride raw materials [53], as eliminating hydroxyl groups diminishes loss (at specific wavelengths) and is therefore favorable for the commercialization of tellurite glass fibers.

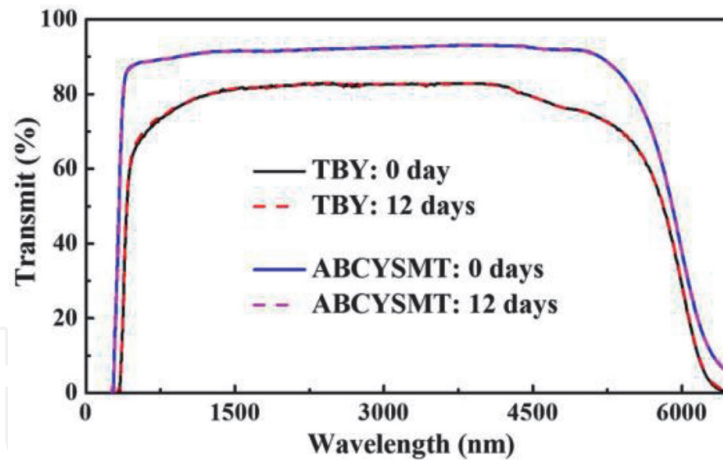


**Figure 3.**  
 Transmission spectra of two kinds of tellurite glasses before and after dipping in water [52].

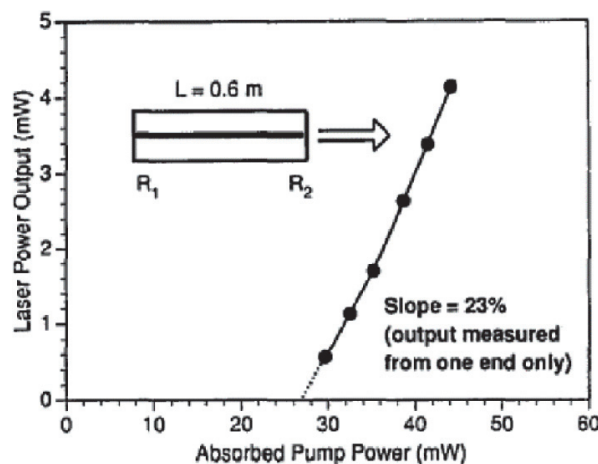


**Figure 4.**  
 The relationship between the laser output power and the pump power ( $R_1 = R_2 = 11.9\%$ ) in  $\text{Nd}^{3+}$ -doped tellurite fiber. Considering that the laser output power at both ends of the fiber is the same, the total slope efficiency should be 46% [12].

With the above advantages coupled with excellent thermal stability, tellurite glass preforms could be handled with relative ease for casting [24, 53], drilling [54], and extrusion techniques [55], providing precursors for tellurite fiber-based nonlinear optical processing [56] and fiber lasers.

In 1994, Wang et al. successfully prepared a  $\text{Nd}^{3+}$ -doped tellurite single-mode fiber for the first time. The numerical aperture of the fiber was determined as 0.21. The laser resonator was formed as a consequence of multiple Fresnel reflection ( $\sim 11.9\%$ ) from the end surfaces of the fiber. A laser with a wavelength of  $0.818 \mu\text{m}$  was used as the pump source. A laser output with a wavelength of  $1.061 \mu\text{m}$  was obtained from a 0.6 m long fiber, with a laser threshold of  $\sim 27 \text{ mW}$ . When only single ended output is considered, the slope efficiency of the laser was 23%, as shown in **Figure 4** [12].

In 1998, Ohishi et al. used a 0.9-m-long  $\text{Er}^{3+}$ -doped tellurite fiber as the gain medium to construct a ring laser cavity. When the pump power was 300 mW, a continuous tunable laser output covering 1529–1623 nm was obtained using a tunable filter. A 2.4-m-long  $\text{Er}^{3+}$ -doped tellurite fiber was used as the gain medium to obtain laser output at  $\sim 1624.5 \text{ nm}$ , with a slope efficiency of 3.6% as shown in **Figure 5** [57].

In 2011, Dong et al. demonstrated a high-performance  $\text{Er}^{3+}/\text{Ce}^{3+}$  co-doped tellurite fiber amplifier and tunable fiber laser using a dual-pumping scheme.



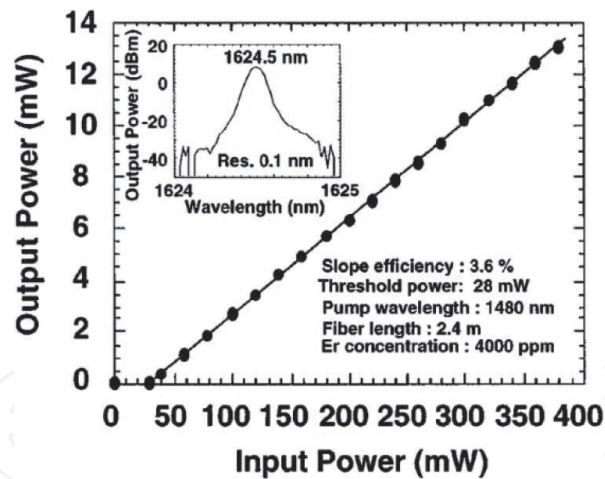


**Figure 5.** Laser characteristics of a tellurite-based fiber laser operating in the 1625 nm band. The inset shows the lasing spectrum of the fiber laser [57].

The short 22 cm fiber exhibits a net gain of 28 dB at 1558  $\mu\text{m}$ , a wide positive net gain bandwidth of 122  $\mu\text{m}$ , and a noise figure of 4.1 dB. As shown in **Figure 6**, a widely tunable  $\text{Er}^{3+}/\text{Ce}^{3+}$  co-doped tellurite fiber ring laser with a tuning range of 83  $\mu\text{m}$  was demonstrated [58].

In 2012, M. Oermann et al. fabricated  $\text{Er}^{3+}$ -doped tellurite microstructured fibers with three air holes using an extruding method. The resulting fibers are shown in cross section in **Figure 7**. The core diameter of the fiber was about 1.5  $\mu\text{m}$ , the loss was 1.3 dB/m, and the doping concentration of  $\text{Er}^{3+}$  was 0.022 mol %. A 2.2-m-long  $\text{Er}^{3+}$ -doped tellurite microstructure fiber was used as the gain medium to construct the laser cavity and was pumped using a 976 nm laser source. As shown in **Figure 8**, its threshold power is only 1.5 mW, and its slope efficiency reaches 13% [59].

In the same year, Chillcce et al. fabricated an  $\text{Er}^{3+}$ -doped tellurite microstructured fiber using the stack-and-draw technique. They demonstrated laser emission using a simple double-pump configuration with two sources at 980  $\mu\text{m}$ . The fiber core had a hexagonal structure as shown in **Figure 9**, the  $\text{Er}_2\text{O}_3$  doping concentration was 7500 ppm, and the background loss of the resulting microstructured fiber was 0.2 dB/cm at  $\sim 1117 \mu\text{m}$ . Two short segments of fiber of 5 and 12 cm generated laser emissions at 1532.3, 1536.3, and 1558.5  $\mu\text{m}$ , as shown in **Figure 10**. The maximum optical signal-to-noise ratio (OSNR) obtained was 21.2 dB [60].

In 2014, Yao et al. fabricated microstructured fibers consisting of a solid core surrounded by six air holes using a rod-in-tube method. A maximum unsaturated power of 9 mW laser operating at  $\sim 1872 \mu\text{m}$  was obtained in a  $\text{Tm}^{3+}$ -doped 2.8 cm

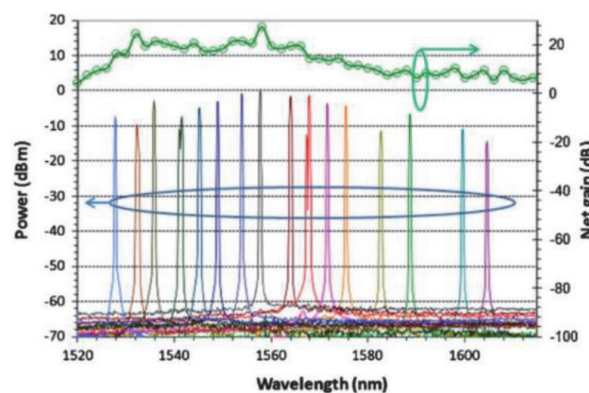


**Figure 6.** Output spectra of the  $\text{Er}^{3+}/\text{Ce}^{3+}$  co-doped tellurite fiber ring laser [58].

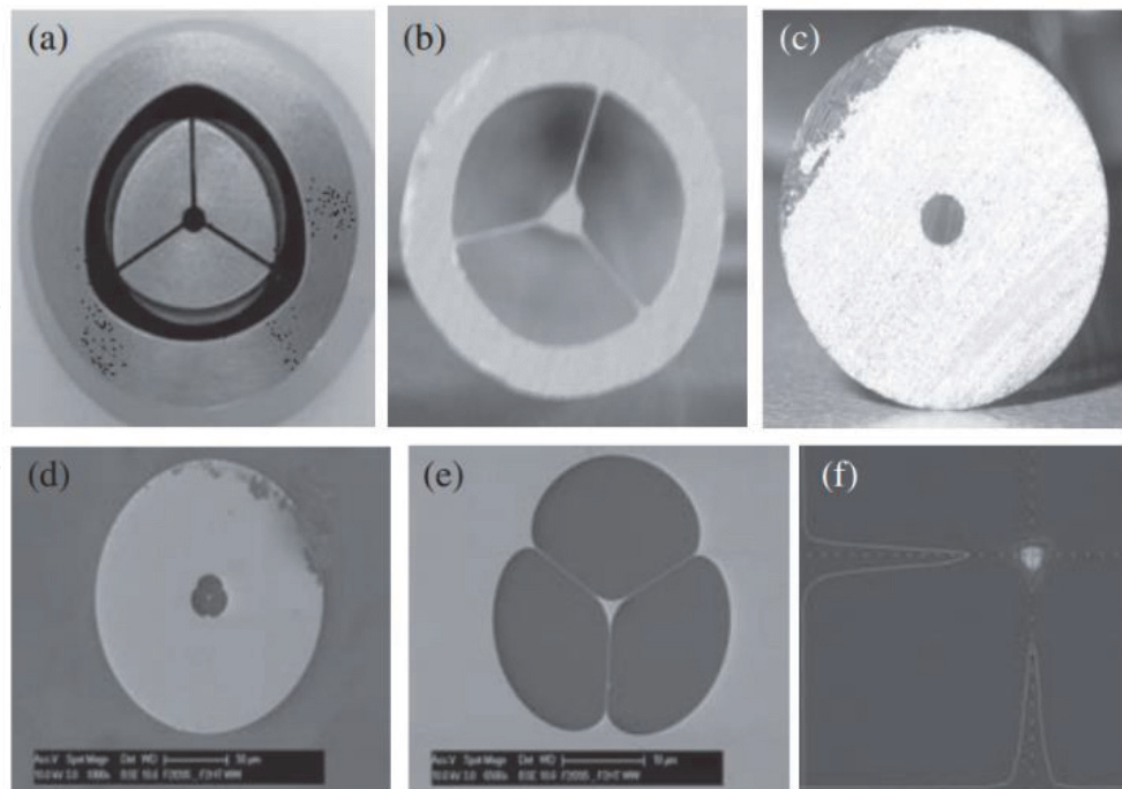


**Figure 7.** Photographs of (a) stainless steel die exit used for the extrusion of the structured preform and (b and c) the extruded structured and jacket preforms, respectively. SEM images of the (d) fabricated fiber cross section, (e) enlarged SEM image of the fiber's core and cladding, and (f) beam profile of the laser mode emitted from the output of the fiber [59].

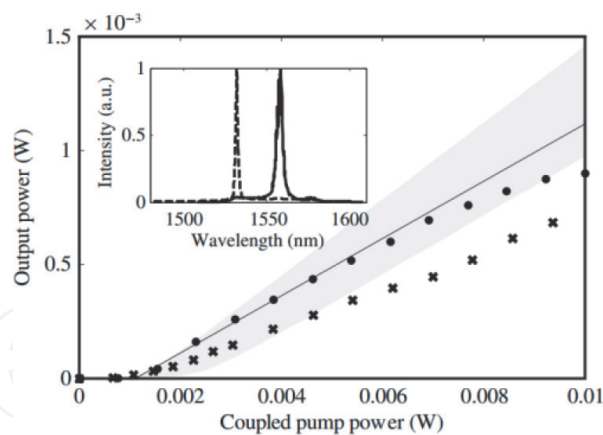


**Figure 8.** Fiber laser output plotted against the coupled pump power for a fiber length of 2.2 m (circles). The figure inset is a plot of the laser output spectrum for 5 mW of coupled pump power into the 1 m (dashed) and 2.2 m (solid) lengths of fiber [59].

long microstructure fiber with a slope efficiency of  $\sim 6.53\%$  and a threshold power of  $\sim 200$  mW. The results shown in **Figure 11** indicate that the  $\text{Tm}^{3+}$ -doped tellurite microstructure fiber is a promising material for achieving a compact  $2 \mu\text{m}$  output fiber laser [61].

In 2015, Meng et al. used a 22-cm-long  $\text{Tm}^{3+}/\text{Ho}^{3+}$  co-doped tellurite fiber to obtain a continuous laser output with a maximum output power of 8.34 mW and a wavelength of 2065 nm when the pump power was 507 mW, as shown in **Figure 12**. The slope efficiency was 2.97% [62].

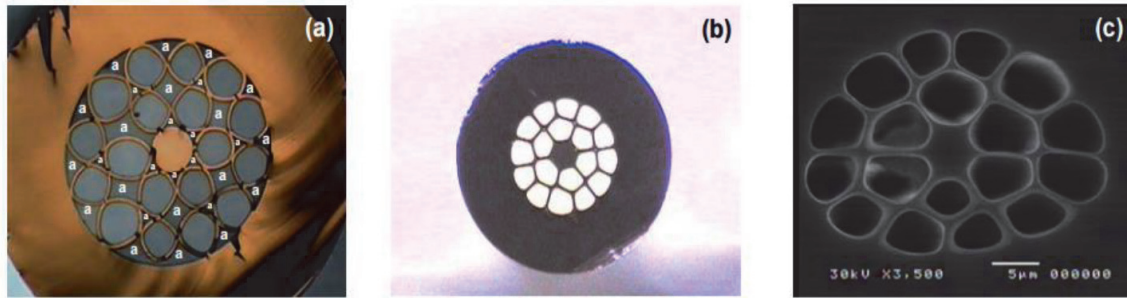


**Figure 9.** (a) Preform with the first clad before eliminating the air trapped. The air regions are indicated with a white “a”. (b) Preform without the air trapped. (c) Scanning electron microscope image of the microstructure fiber [60].

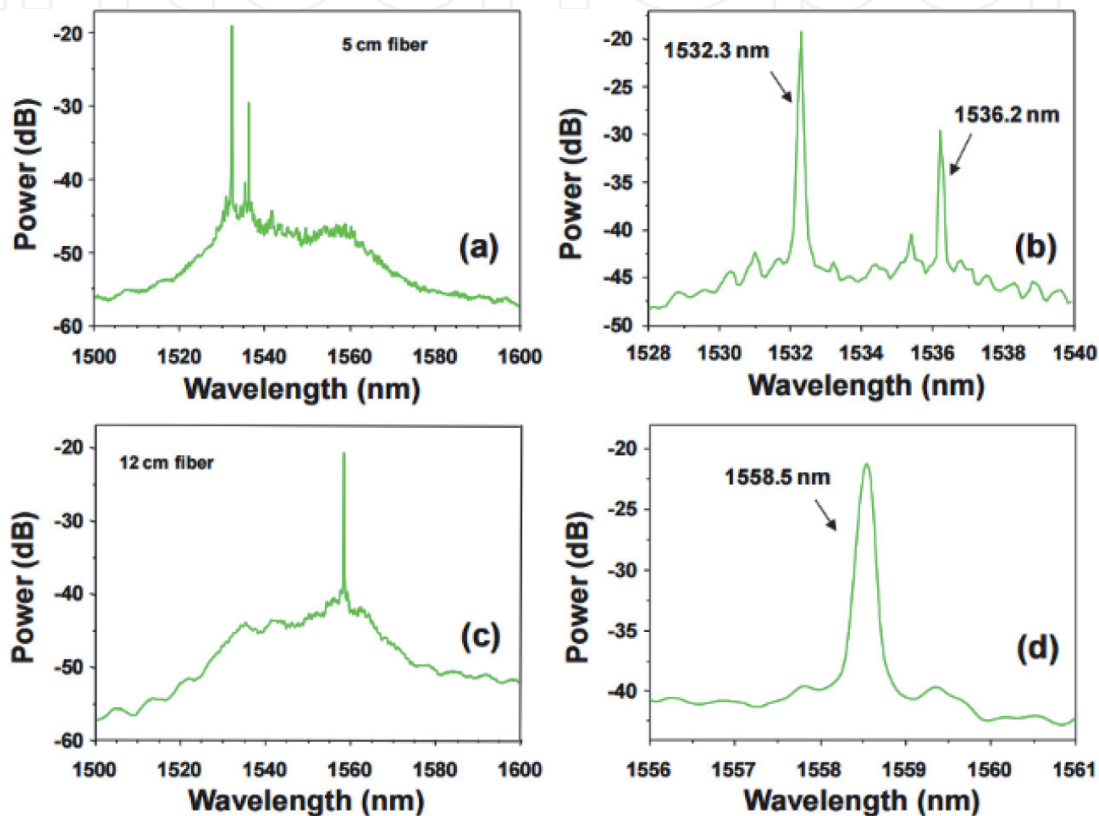


**Figure 10.** Laser emission spectra. (a) 5 cm fiber segment. (b) A zoom of the emission region observed in (a). (c) 12 cm fiber segment. (d) A zoom of the emission region observed in (c) [60].

## 2.2 Tellurite fiber-based supercontinuum light source

The supercontinuum (SC) light source is defined as a broadband laser source whose output spectrum is greatly broadened through the interaction of nonlinear effects and dispersion when a high peak power pulsed laser output (e.g., a soliton pulse) propagates in nonlinear optical medium. The SC spectra generated in transparent materials do not usually originate from a single nonlinear process—typically the initiated self-phase modulation (SPM) modulates the phase of the input laser, and then other nonlinear effects including cross-phase modulation (XPM), stimulated Raman scattering (SRS), four-wave mixing (FWM), soliton self-frequency shifting (SSFS), etc. broaden the output frequency (wavelength) spectrum [63]. The first observation and application of SC spectra were obtained in solids and liquids [64–66], but recent investigations and applications of SC light sources have utilized optical fibers including single-mode and microstructured fibers [67]. The latter is a widely used medium due to its unique geometry and low transmission loss



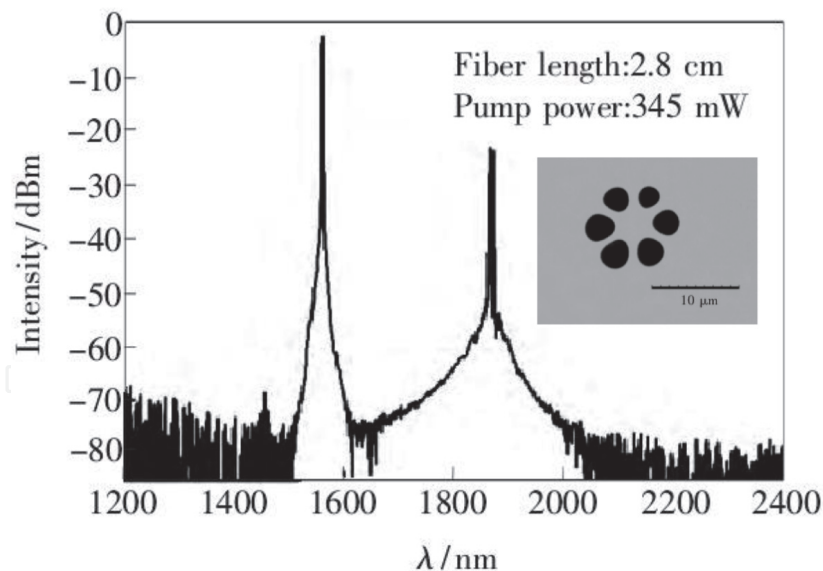


**Figure 11.**  
*Laser spectrum of fiber laser pumped by 1560 nm band fiber laser. The figure inset shows cross section of  $Tm^{3+}$ -doped TZNB microstructure fiber [61].*

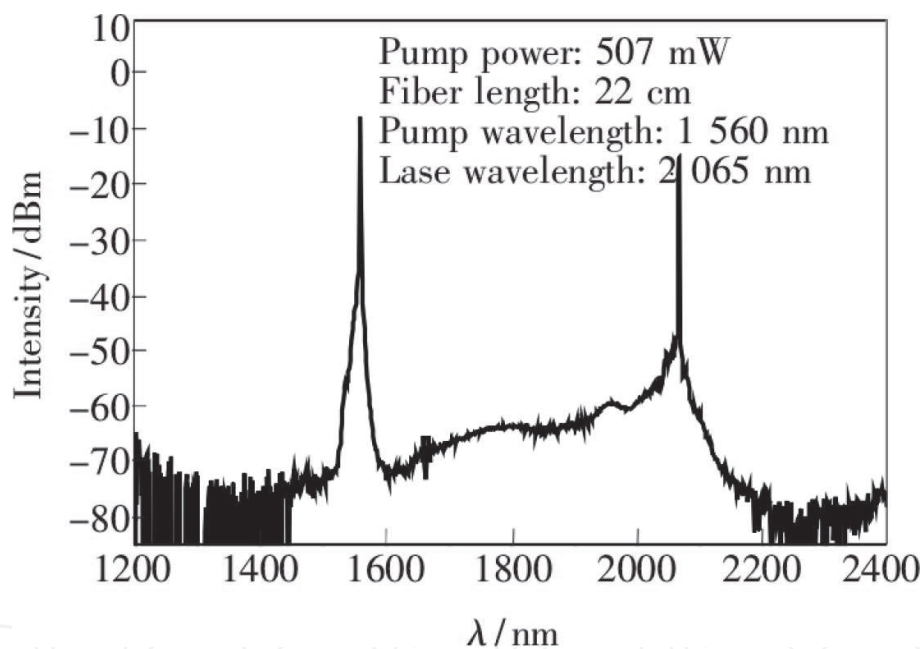


**Figure 12.**  
*Spectrum of the fiber laser pumped by 1560 nm band fiber laser [62].*

that can accumulate the power intensity of pump sources and provide adequate interaction length to facilitate the occurrence of the nonlinear processes. In 2005, half the Nobel Prize in Physics were awarded for the development of optical frequency combs that was generated from the SC coherent light source employing microstructured silica fiber. SC light sources based on silica microstructured fiber with outputs spanning from the ultraviolet to the near infrared spectral regions have been widely commercialized by major optics firms, such as American Corning corporation, Fujitsu and Nippon of Japan, Korea's ETRI and so on.

The 2–5- $\mu$ m-mid-infrared region is the typical wavelength range corresponding to the “atmospheric optics window,” the “molecular fingerprint region,” and “strong absorption band of hydroxyl and amino groups.” Therefore, SC light sources in this region offer great possibilities for optical telecommunication, remote sensing, atmospheric pollution monitoring, molecular spectroscopy, medical

diagnosis, hyperspectral imaging, laser surgery, and IR opto-electric countermeasures [63, 68], all of which greatly attracted intense worldwide research interest over the past two decades [69–71]. There are several requirements of nonlinear fibers used for 2–5  $\mu\text{m}$  SC light sources, e.g., they must be transparent within the 2–5  $\mu\text{m}$  window, they must have a relatively high laser damage threshold for potentially high-power light transmission, they should have a high nonlinear refractive index, and they need to be fabricated based on mature processing technology. Silica is not a candidate material for generating SC spectra at wavelengths longer than 2.2  $\mu\text{m}$ , due to its high intrinsic loss and relatively low nonlinear parameters. Alternatively, soft glass fibers, mainly including fluoride, tellurite, and chalcogenide glass fibers, are being investigated to develop SC light sources in the 2–5  $\mu\text{m}$  spectral region and have achieved remarkable progress to date with their broad IR transparency range as well as prominent optical nonlinearity.

Among the soft glass materials investigated, tellurite glass provides many several attractive features for use in high-power SC light sources. These include a broad IR transmission window (0.3–7  $\mu\text{m}$ ) that can be matched with fluoride glass while possessing lower intrinsic losses than chalcogenide glass and possessing the highest optical damage threshold than other soft glass materials. Moreover, with outstanding thermal and chemical stability, tellurite glass can be drawn as microstructured fiber from a preform constructed using the rod-in-tube method or extrusion technique. The dispersion profile and nonlinearity of the fabricated fiber can be readily optimized. In the past two decades, much effort has been concentrated on fabricating a microstructured tellurite fiber for SC generation.

Kumar et al. prepared low-loss tellurite microstructured fiber for the first time using an extrusion and rod-in-tube method, whose minimum loss was 2.3 dB/m at 1055 nm [72]. Photographs of the fiber are shown in **Figure 13**. In such a microstructured fiber with 1.02 m length, they studied the stimulated Raman scattering generation pumped using a 1064 nm pulsed laser.

In 2008, Domachuk et al. generated a SC spectrum with a broad bandwidth covering the spectral range 789–4870 nm in tellurite microstructured fiber pumped using a 1550 nm pulsed laser [73]. As shown in **Figure 14**, the fiber core was surrounded by six large diameter air holes to achieve strong light confinement, and the calculated nonlinear waveguide coefficient at 1550 nm was  $596 \text{ km}^{-1} \text{ W}^{-1}$ ,

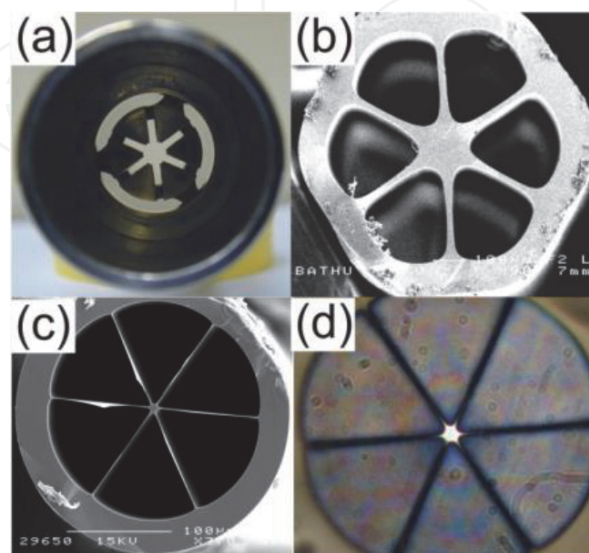


**Figure 13.**

(a) The cross section of the die used for extrusion. (b) Electron micrograph of an extruded tellurite preform, with outer diameter 1 mm. (c) Electron micrograph of tellurite PCF. (d) Transmission view of a tellurite PCF as seen in microscope [72].



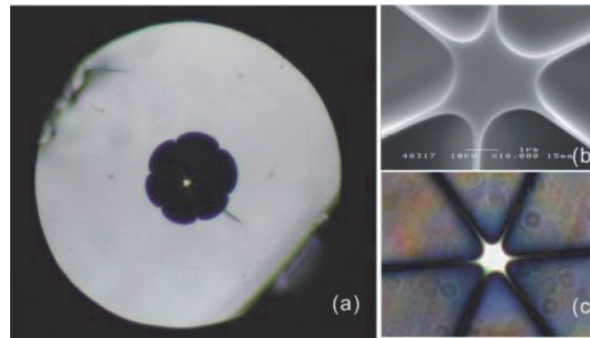


**Figure 14.** Picture as seen in optical microscopy (a and c) and cross section profile of the tellurite PCF in electron microscopy (b). Scale bar in (b) is 1  $\mu\text{m}$  [73].

which broadened the SC spectrum spanning two and a half optical octaves in the fiber having only a length 0.8. Such a short fiber length results in flatter SC spectra, lower dispersion, and reduced material absorption at longer wavelengths.

In 2008, Feng et al. fabricated a large-mode-area tellurite holey fiber from an extruded preform, with a core diameter of  $\sim 80 \mu\text{m}$ , attenuation of 2.9 dB/m at 1.55  $\mu\text{m}$ , and zero-dispersion wavelength (ZDW) at 2.15  $\mu\text{m}$  (**Figure 15**) [74]. Using such microstructured fiber with a 9 cm length, a broadband SC spanning of 0.9–2.5  $\mu\text{m}$  was achieved.

In 2009, Liao et al. fabricated the hexagonal core fiber (**Figure 16**) for the first time [75]. They studied the SC generation in such a fiber of 6 cm length pumped by a 1557 nm femtosecond laser and with a 30-cm-long fiber pumped using a 1064 nm picosecond fiber laser. Additionally, they demonstrated that the holey region has an important influence on the dispersion, nonlinear coefficient, and SC generation.

In 2010, a 36-cm-length tellurite microstructured fiber with four holes [76] was used to generate a flattened SC spectrum spanning from 900 to 2800 nm (**Figure 17**) and was pumped using a 1550 nm pulsed laser. The calculated nonlinear coefficient at 1550 nm was  $539 \text{ km}^{-1} \text{ W}^{-1}$  [76].

In 2012, Savelii et al. prepared a low-loss suspended-core tellurite fiber, from which they generated a 0.75–2.8  $\mu\text{m}$  SC spectrum when pumped at 1745 nm [77]. And in 2015, Belal et al. generated SC spectra extending to 3  $\mu\text{m}$  in a suspended-core tellurite fiber. Their numerical study show that the structure of the fiber can have a significant impact on the dispersion profile and hence the nonlinear processes and SC broadening [78].

In 2013, Klimczak et al. reported a breakthrough in the design of optical fiber transverse structure. They produced a novel, regular hexagonal-lattice tellurite photonic crystal fiber (PCF) as shown in **Figure 18** [79]. Pumping the 2-cm-long

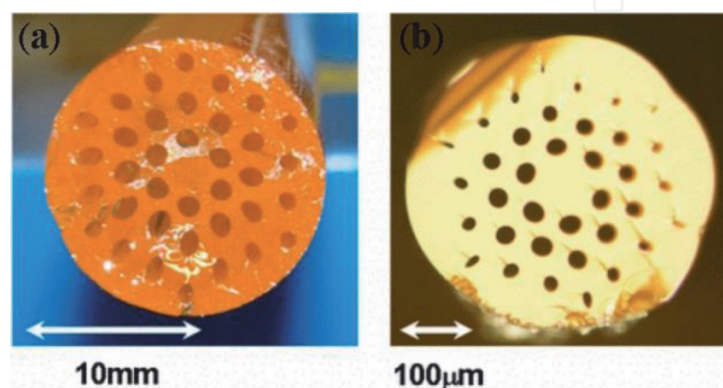


**Figure 15.** Optical photographs of the cross-sectional views of (a) the extruded tellurite preform and (b) the resulting tellurite holey fiber with 410  $\mu\text{m}$  outer diameter [74].

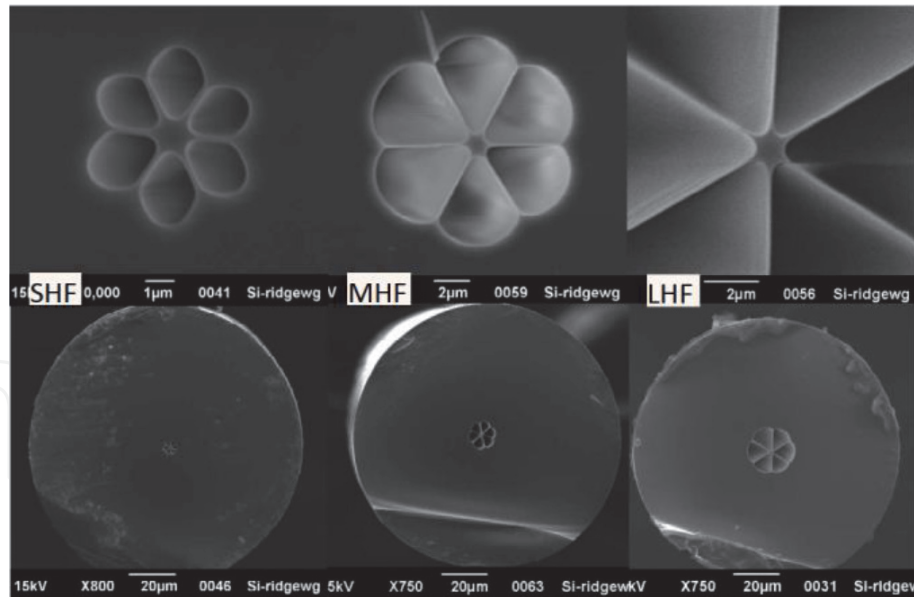


**Figure 16.** Scanning electron microscope (SEM) images of the fibers [75].

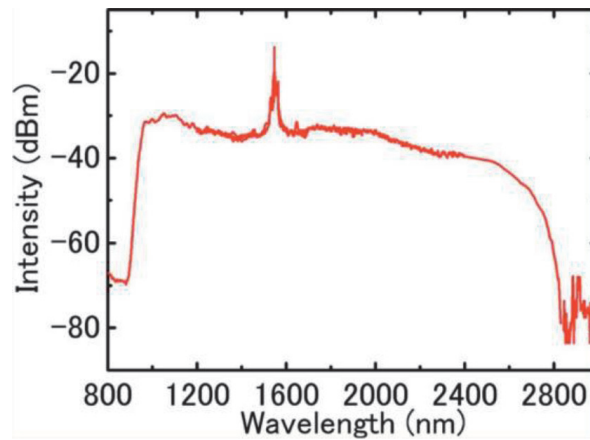


**Figure 17.** SC spectrum generated from the tellurite fiber when the peak power of the pump laser is fixed at 3.9 kW [76].

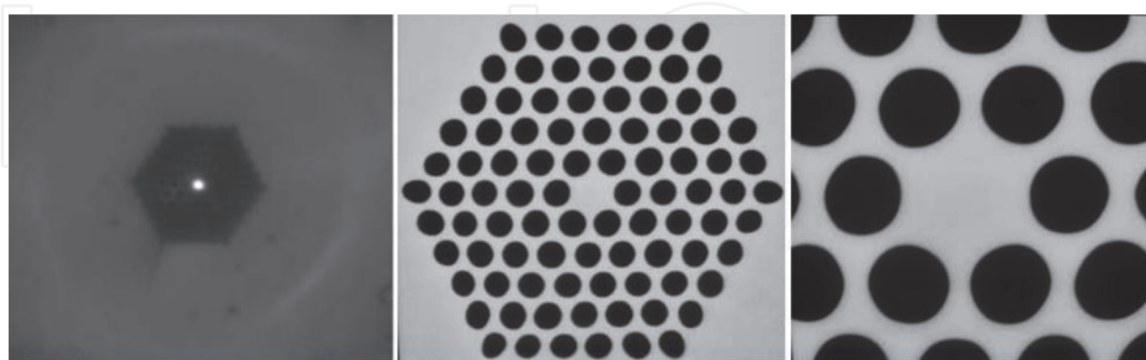


**Figure 18.** Microstructure of tellurite PCF: close-up picture of the structure with propagating mode as seen in a CCD camera, and SEM images of photonic structure [79].

PCF with 150 fs/36 nJ/1580 nm pulses, they achieved an output of 800–2500 nm SC spectrum that is comparable to that generated in suspended-core tellurite PCF pumped at wavelengths over 1800 nm.

Yao et al. proposed a novel fluorotellurite fiber with the composition  $65\text{TeO}_2\text{-}25\text{BaF}_2\text{-}10\text{Y}_2\text{O}_3$  (TBY) [80]; the authors claimed further improvement in the

performance of tellurite fiber-based MIR laser sources. BaF<sub>2</sub> was included for the purpose of reducing the OH— content, and the introduction of Y<sub>2</sub>O<sub>3</sub> was for better thermal stability in fiber drawing process as well as providing a higher glass transition temperature raised by the high melting temperature of Y<sub>2</sub>O<sub>3</sub>. In 2016, Wang et al. achieved SC generation extending from 0.47 μm to 2.77 μm (zero-dispersion wavelength at 1730 nm) using a tapered TeO<sub>2</sub>-BaF<sub>2</sub>-Y<sub>2</sub>O<sub>3</sub> (TBY)-based microstructured fiber whose core was surrounded by six air holes [81].

Tellurite microstructured fibers with dispersion modification and nonlinear coefficient enhancement have been widely studied and applied for SC generation, and significant progress has been achieved over the last 10 years. However, the air holes present in microstructured fibers readily accommodate moisture and dust particles from the atmosphere, which lead to incremental losses, which act to deteriorate the SC output. In addition, the performance of tellurite microstructured fiber for high-power output in the mid-IR SC is not satisfactory, because the thermal conductivity of the air holes and the core of microstructure fiber greatly differ, and hence means that heat dissipation is a significant problem of high-power light transmission in the fiber. Solid-state tellurite fibers (comprising a solid core and cladding with no air holes) have therefore become the nonlinear medium of choice for high-power mid-infrared SC light sources [82].

Hydroxyl ions have deleterious broad absorption peaks centered at ~3.3 μm and ~4.3 μm, which hinder the tellurite fiber from extending its spectrum to the multiphonon edge (5 μm). In 2013, Thapa et al. of NP Photonics Incorporation developed ultra-low-loss solid-core tellurite fibers which eliminate almost all molecular species, especially hydroxyl ions [83]. Using a 1922-nm all-fiber-based mode-locked fiber laser oscillator, a 1–5 μm SC spectrum shown in **Figure 19b** was generated in a tellurite fiber with a W-type (**Figure 19a**) index profile for strong light confinement, and the ZDW shifted from 2.5 μm to ~1.9 μm. It was argued that the broadened anti-Stokes wavelength portion originated from self-phase modulation (SPM) and the long wavelength portion with increased power originated from the generation of a Raman soliton because of the self-frequency Raman shift. In the same year, Savellii et al. reported SC generation extending from 840 nm to 3000 nm in a low-loss suspended-core tellurite fiber with different lengths (**Figure 20**), pumped at its anomalous dispersion regime at 1745 nm [54]. It was found that the introduction of fluoride ions into the tellurite glass reduced the OH— content and resulted in a fiber that was still transparent at 4.1 μm.

The W-type index profile makes it possible to tailor the ZDW, and this fiber can be fusion spliced to robust step-index silica fiber with relative ease. In 2016

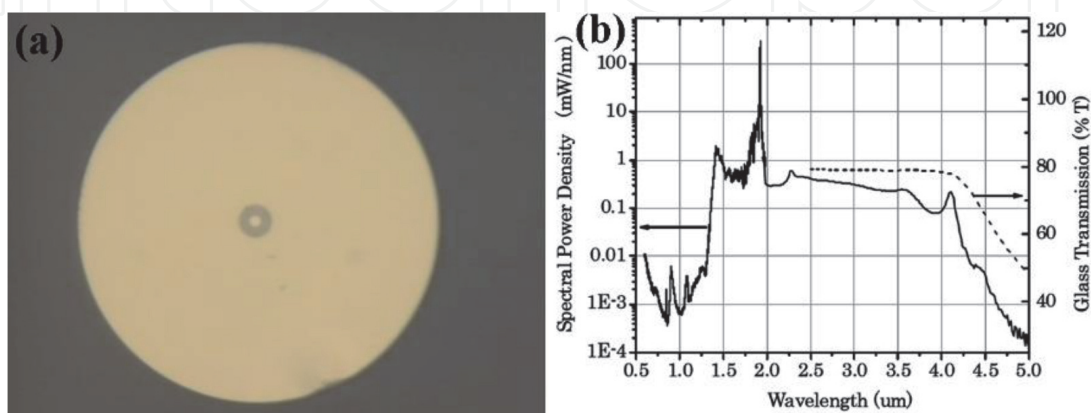


**Figure 19.**

(a) Cross section of the W-type tellurite fiber. (b) SC spectra in W-type proprietary tellurite fiber pumped by 3 W of ~20 ps pulses from a 32 MHz repetition rate amplified mode-locked laser at 1.92 μm. (Note: dotted line is the transmission measured in the corresponding 1-cm-thick tellurite glass sample.) [83].



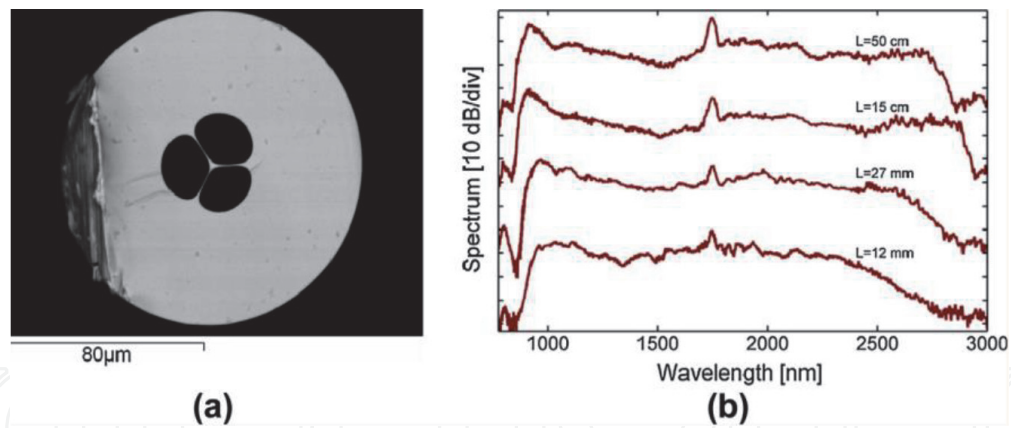


**Figure 20.**

(a) SEM picture of the cross section of the fiber. (b) SC spectra generated from the suspended-core tellurite fiber with different lengths [54].

Kedenburg et al. studied SC generation spanning 2.6–4.6  $\mu\text{m}$  in low-loss W-type index tellurite fiber with a length of 15 cm [84]. Additionally, they studied the variation of spectral bandwidth with core diameter, pump wavelength, length of fibers, and pump power. In 2017, Kedenburg et al. studied the effects of the core size, pump wavelength, and fiber length on SC generation in a robust step-index tellurite fiber, and they achieved broadband SC generation spanning 1.3–5.3  $\mu\text{m}$  in the fiber with a length of 9 cm and a core diameter of 3.5  $\mu\text{m}$ , when pumped using a 2.4  $\mu\text{m}$  femtosecond pulsed laser [85].

In 2016, Shi et al. prepared a solid-state tellurite optical fiber with a numerical aperture (NA) of 0.21 and a core diameter of 12  $\mu\text{m}$  [86]. **Figure 21(a)** shows a micrograph of the end face of the fiber. They studied the SC generation in the fiber which was 0.8 m-in length. **Figure 21(b)** shows the spectrum of the pump laser and SC output in the fiber when different pump powers were used. When the pump power was 9.8 W, the power spectral density of the SC spectrum in the wavelength range of 1975–3000 nm is above 5 dBm/nm. In this investigation, the maximum output power of the SC light source was 5.1 W, and the power of the spectrum at wavelengths longer than 2.5  $\mu\text{m}$  was about 2.1 W.

In 2017 Jia et al. obtained a stable 4.5 W SC output spanning 1017–3438 nm, using a TBY-based 60-cm-long all-solid fluorotellurite fiber fabricated using the rod-in-tube method. The fiber was pumped using a 2  $\mu\text{m}$  femtosecond fiber 10.48 W output power laser and thus demonstrated the capability of all-solid fluorotellurite fibers for

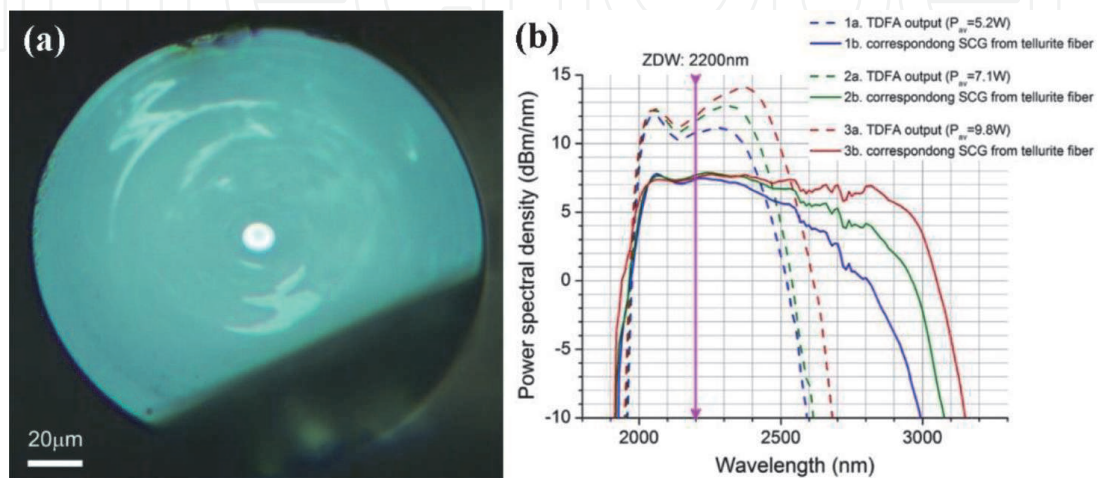


**Figure 21.**

(a) Photograph of the tellurite fiber. (b) Spectrum of thulium-doped fiber amplifier (T DFA) and the SC spectrum generated from the tellurite fiber, pumped by various power: 5.2 W, 7.1 W, and 9.8 W [86].

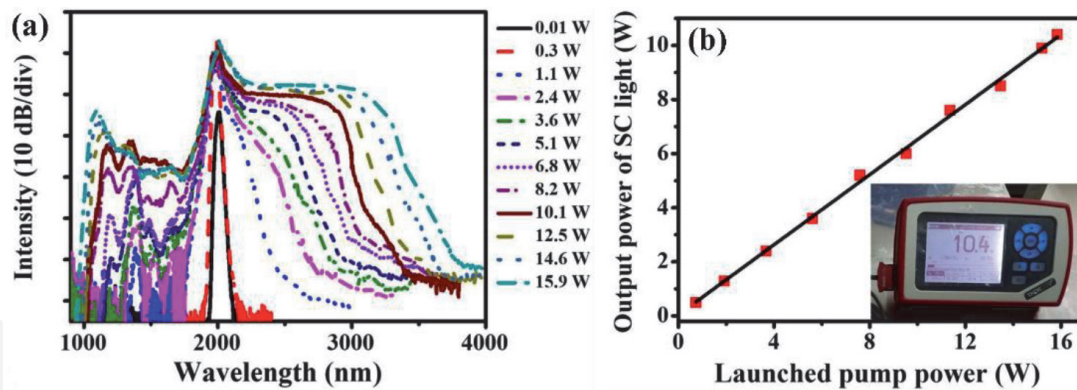


**Figure 22.** (a) Dependence of the measured SC spectra generated from 60-cm-long fluorotellurite fiber on the average power of the 1980 nm femtosecond fiber laser. (b) The dependence of the SC average power on the pump power. Inset: photograph of the power meter when the mid-IR SC laser source is operating at the output power of 10.4 W [52].

use as high-power mid-IR SC light sources [87]. The same authors used a tapered all-solid fluorotellurite fiber with ultra-high NA to generate an SC output spectrum covering the entire 0.4–5  $\mu\text{m}$  transmission window and pumped using a 1560-nm mode-locked fiber laser [88]. Yao et al. achieved stable 10.4 W SC generation in the wavelength ranging from 947 to 3934 nm from a TBY-based all-solid fluorotellurite fiber when pumped using a high-power 1980 nm femtosecond fiber laser [52]; when the average pump power was increased to 1.1 W, large spectral broadening occurred as shown in **Figure 22(a)**. Because the fiber was pumped at anomalous dispersion regime, the spectral broadening for a pump power of  $\geq 1.1$  W originated from the SPM, the formation of higher-order soliton, soliton fission, soliton self-frequency shift (SSFS), and the generation of blue-shifted dispersive waves. The average output power of the SC laser source increases linearly with the average pump power (**Figure 22(b)**), and the corresponding optical-to-optical conversion efficiency was measured to be as high as 65%. The successful achievement of a 10 W output power level represented a significant breakthrough in all-solid fluorotellurite fiber, demonstrating its bright future for high-power MIR SC light sources.

### 3. Tellurite glass-based microcavity lasers

#### 3.1 Experimental preparation of tellurite glass microcavities

Over the past few decades, research interest in microsphere resonators has grown rapidly. For a microsphere resonator, the pump light can be coupled into the microsphere through a tapered optical fiber or via free space. Most current microsphere resonators are fabricated from the silica optical fiber, but it is also possible to fabricate microsphere resonators from compound glass materials (such as tellurite glass) other than silica. At present, the principal method used for making microsphere cavities is based on melting of the glass materials, which uses the surface tension of molten glass to form the microsphere when suspended at the tip of a fiber. There are two common methods for the preparation of tellurite glass microsphere cavities, one is to melt glass fiber and the other is a powder floating method.

##### 3.1.1 Melting glass fiber method

Most glass microsphere cavities are prepared using a  $\text{CO}_2$  laser, arc discharge, or high temperature ceramics to melt glass fibers. These methods have also been



widely applied for fabricating tellurite glass microsphere cavities and other compound glass microsphere cavities resulting in a good shape and high Q factor. The fabrication method using a CO<sub>2</sub> laser is described here.

A schematic diagram of the experimental setup for manufacturing a microsphere resonator is shown in **Figure 23**. The main positioning and alignment instrument used in the experiment was a precision three-dimensional (3D) translation stage, a continuous CO<sub>2</sub> laser with an output wavelength of 10.6 μm, and a ZnSe lens for focusing. The experimental step for fabricating the tellurite microsphere resonator was divided into three stages. In the first step, the tellurite fiber was mounted vertically on the 3D translation stage and a weight hung at the end of the fiber. The ZnSe lens was used to focus the laser beam on the tip of the tellurite fiber, causing it to absorb the incident light which resulted in a temperature rise. The glass softened and gradually stretched into a tapered fiber under the influence of the weight. The heating was terminated when the waist diameter of the tapered fiber reached around 30 μm. In the second step, the tapered fiber was accurately cleaved at the waist region to obtain a half-tapered fiber. In the third step, using a ZnSe lens once more to focus the laser beam on the end of the half-tapered fiber, the tellurite microsphere was formed at the fiber end due to the surface tension acting

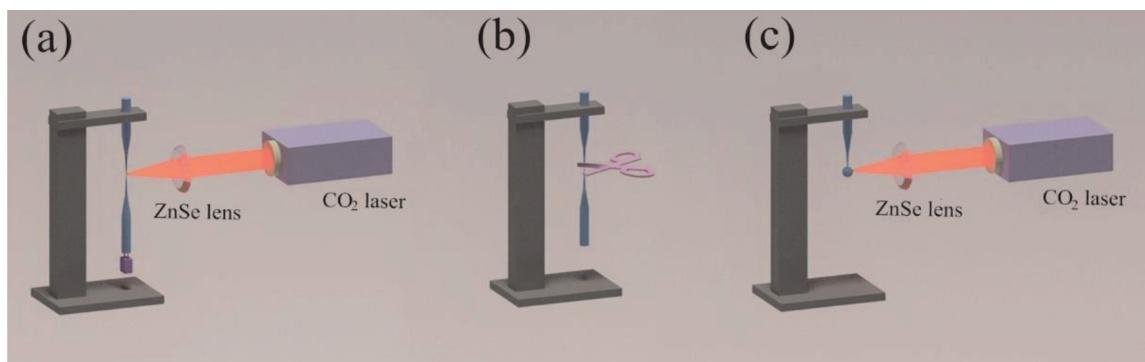


**Figure 23.** Schematic diagram of the experimental setup for making a tellurite glass microsphere. (a) A ZnSe lens is used to focus a CO<sub>2</sub> laser beam on the tellurite fiber. (b) The waist region of tapered fiber is cleaved. (c) A tellurite microsphere is obtained by focusing a CO<sub>2</sub> laser beam on the end of the cleaved tapered [92].

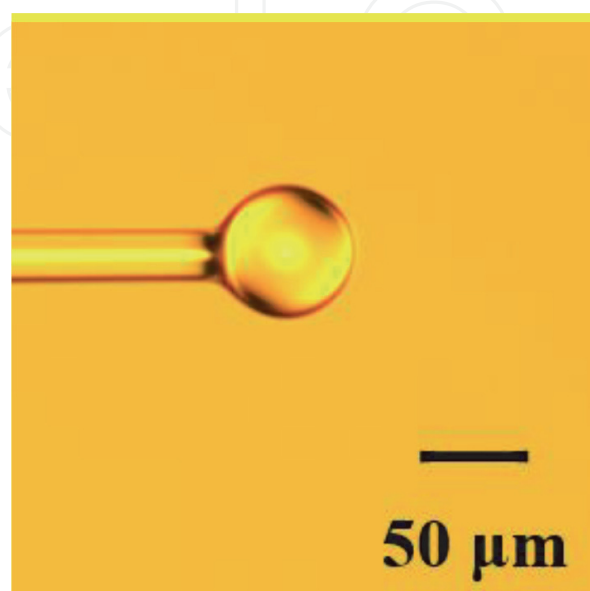


**Figure 24.** Microscope image of tellurite microsphere made with CO<sub>2</sub> laser.

on the molten glass. A microscope image of a tellurite microspheres fabricated in this manner is shown in **Figure 24**.

Although the resulting microsphere cavity made of molten glass fiber includes a glass fiber attached at a pole of the sphere, the light field is mainly concentrated around the equatorial plane of the microsphere cavity, and hence the loss induced by the fiber to the whispering gallery mode (WGM) resonance is negligible [89, 90]. In general, the fiber rods are only used to hold the microspheres in place and to facilitate light coupling. However, in recent years, some other uses of fiber rods have attracted increasing attention. In 2017, Murphy et al. [91] reported an alternative method for precise coupling control using the fiber rod. In the experiment, 980 nm laser light was input into the fiber rod, and the coupling distance between the microsphere cavity and the tapered fiber was precisely controlled by heating the connection between the microsphere and the fiber rod using the 980 nm laser. The adjustment range of microsphere cavity position was from  $0.61 \pm 0.13 \mu\text{m}$  to  $3.49 \pm 0.13 \mu\text{m}$ .

### *3.1.2 Powder floating method*

The previously mentioned method for fabricating tellurite glass microspheres was only capable of producing one microsphere at a time, and the powder floating represents an alternative method for preparing glass microspheres in large quantities. In this method, the tellurite glass was ground into powder and poured into a high temperature furnace, which was placed vertically with a proper protective gas (nitrogen or inert gas) from the bottom to top. The tellurite glass powder melts and forms into microspheres due to surface tension at high temperature. In addition, the protective gas reduced the falling speed of the glass powder and increased the exposure time of the powder to the high temperature in the furnace. Additionally, the method isolates the glass powder from the atmosphere [93]. For some glass materials with less stringent experimental requirements, the microspheres can be formed without the use of protective gas [94].

Tellurite microspheres prepared using this method have no attached fiber rods, which is different from melting glass fiber or sol-gel methods. Using the powdered method, a large number of microspheres with different diameters can be prepared simultaneously, which is beneficial to the selection of experimental size and enables the integration and commercialization of the microsphere laser on a mass produced basis. **Figure 25** is a schematic diagram of fabrication of microspheres, and **Figure 26** is a microscope image of the microspheres fabricated using the powder floating method.

## **3.2 Tellurite glass microsphere lasers**

Tellurite glass has emerged as a promising material for use in microsphere resonators in the near infrared wavelength region and tellurite glass microsphere lasers have been widely reported. In 2002, Sasagawa et al. reported continuous-wave oscillation in an  $\text{Nd}^{3+}$ -doped tellurite glass microsphere laser at  $1.06 \mu\text{m}$  for the first time [96]. Tellurite glass microspheres with diameters in the range of  $50 \mu\text{m}$  to a few hundred micrometers were fabricated by melting using a Kanthal wire heater. Resonances were excited in the microsphere pumped using a 800 nm laser, the threshold of the output laser was measured as 81 mW, and the emission spectrum is shown in **Figure 27**.

Later in 2005, an  $\text{Er}^{3+}$ -doped tellurite glass microsphere laser was reported by Peng et al. [97]. The threshold of 1561 nm microsphere laser with 0.5 wt%  $\text{Er}_2\text{O}_3$  doped was measured to be as low as 1.4 mW, and the maximum output power

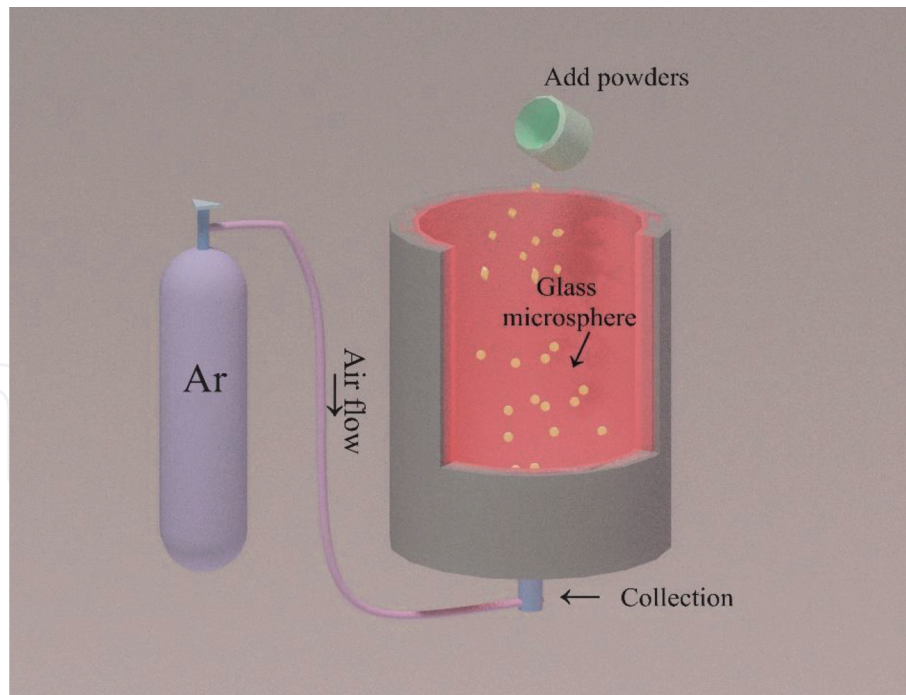


**Figure 25.** Schematic diagram of fabrication of microsphere by powder floating method [95].

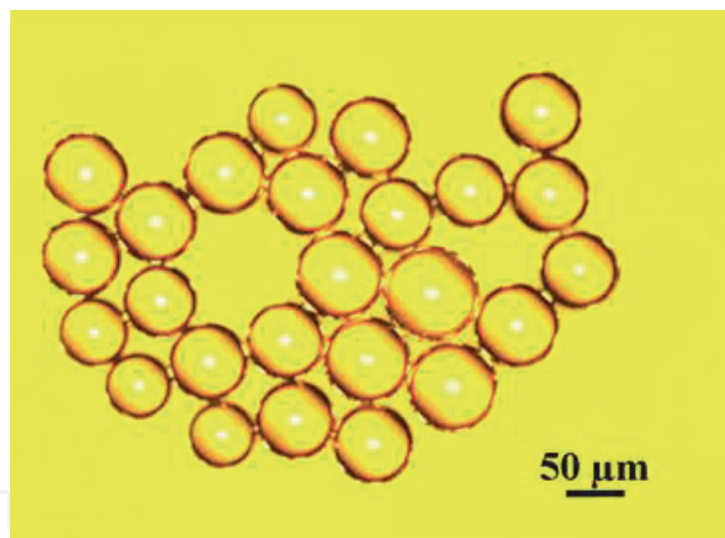


**Figure 26.** Microspheres fabricated by powder floating method.

achieves 124.5  $\mu\text{W}$ . **Figure 28** shows the relationship between the output laser power and the 1480 nm pump power.

The output wavelength of the laser around 1.9  $\mu\text{m}$ , and 1.47  $\mu\text{m}$  band is generated from the transition of  $\text{Tm}^{3+}$  ions:  ${}^3\text{F}_4 \rightarrow {}^3\text{H}_6$  and  ${}^3\text{H}_4 \rightarrow {}^3\text{F}_4$  [98]. Wu et al. proposed a microcavity laser based on a  $\text{Tm}^{3+}$ -doped tellurite glass microsphere at 1.9  $\mu\text{m}$  [99]. However, there are two problems in realizing a laser at the wavelength 1.47  $\mu\text{m}$ . Firstly, the lifetime of the  ${}^3\text{H}_4$  level is shorter than that of the  ${}^3\text{F}_4$  level in  $\text{Tm}^{3+}$  ions, so the transition is sometimes described as self-terminating [100]. Secondly, the glass host material should have very low phonon energy, as in the case of silica and phosphate glass lasers, and amplification is essential. Tellurite and other heavy metal fluoride glasses have been considered as key materials for thulium-doped fiber amplifier operation in the S band, mainly due to their lower phonon energies ( $\sim 580 \text{ cm}^{-1}$ ) [12]. In 2004, Sasagawa et al. solved the population inversion problem in  $\text{Tm}^{3+}$  ions and realized a cascade laser with output wavelengths in the

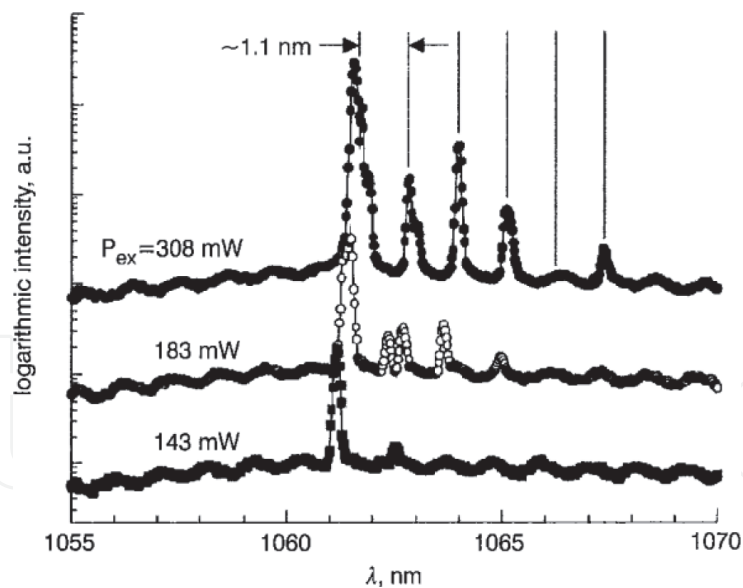


**Figure 27.** Emission spectra for  ${}^4F_{3/2} \rightarrow {}^4I_{11/2}$  transition of  $\text{Nd}^{3+}$  ions in tellurite glass microsphere at various pumping powers [96].

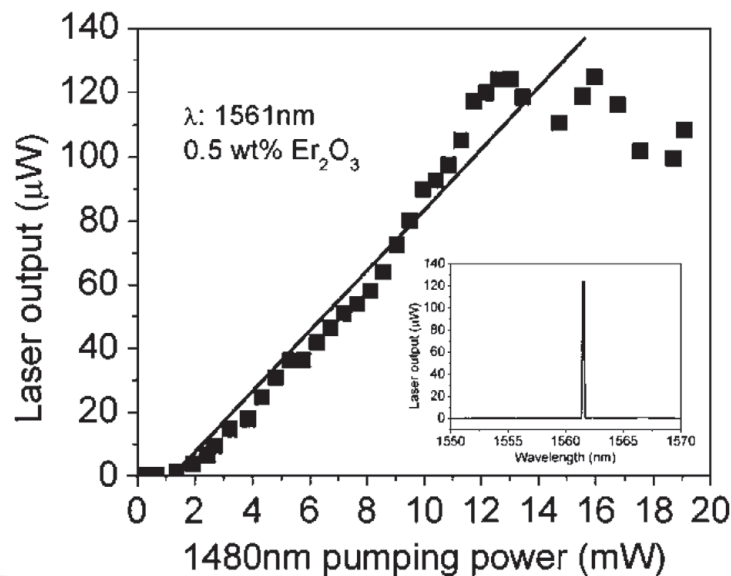


**Figure 28.** The microsphere laser pumped by a 1480 nm laser. The  $\text{Er}_2\text{O}_3$  doping concentration is 0.5 wt%, and the diameter of the microsphere is 32  $\mu\text{m}$ . The maximum output power is 124.5  $\mu\text{W}$ . The inset shows the single-mode profile of this L-band microsphere laser [97].

1.47  $\mu\text{m}$  and 1.9  $\mu\text{m}$  bands using a tellurite glass microsphere [101]. The output spectrum of the  $\text{Tm}^{3+}$ -doped tellurite glass laser is shown in **Figure 29**, which shows the laser emission in the S band and at 1.9  $\mu\text{m}$ . The average output power is plotted as a function of the average pump power in **Figure 30**. The threshold of the laser in the S band is 4.6 mW, while the thresholds measured for 1.9  $\mu\text{m}$  are 3.0 mW and 4.8 mW, respectively. The differential quantum efficiency in the S band and at 1.9  $\mu\text{m}$  were calculated as 1.4% and 1.1% for bidirectional lasing.

In 2019 [3], Li et al. fabricated  $\text{Tm}^{3+}$ - $\text{Ho}^{3+}$  co-doped tellurite glass samples to solve the problem of the population inversion and obtained a 1.47  $\mu\text{m}$  output using a tellurite glass microsphere laser. **Figure 31(a)** shows the output spectrum at 1.47  $\mu\text{m}$  of  $\text{Tm}^{3+}$ - $\text{Ho}^{3+}$  co-doped tellurite glass microspheres when pumped using a 802 nm laser source. It is clear from **Figure 31(b)** that the lifetime of  ${}^3F_4$  energy level is attenuated through the energy transfer process in  $\text{Tm}^{3+}$ - $\text{Ho}^{3+}$  co-doped tellurite



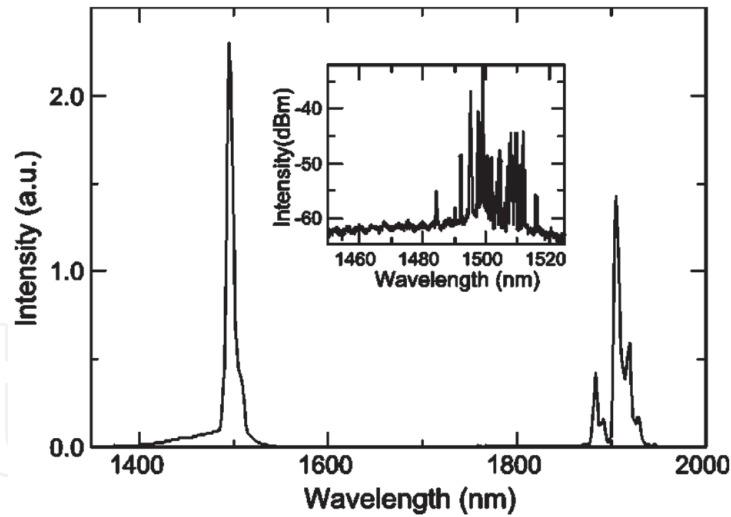


**Figure 29.** Emission spectrum of a  $Tm^{3+}$ -doped tellurite microsphere laser with diameter of  $104 \mu m$ . (Inset) OSA emission spectrum [101].

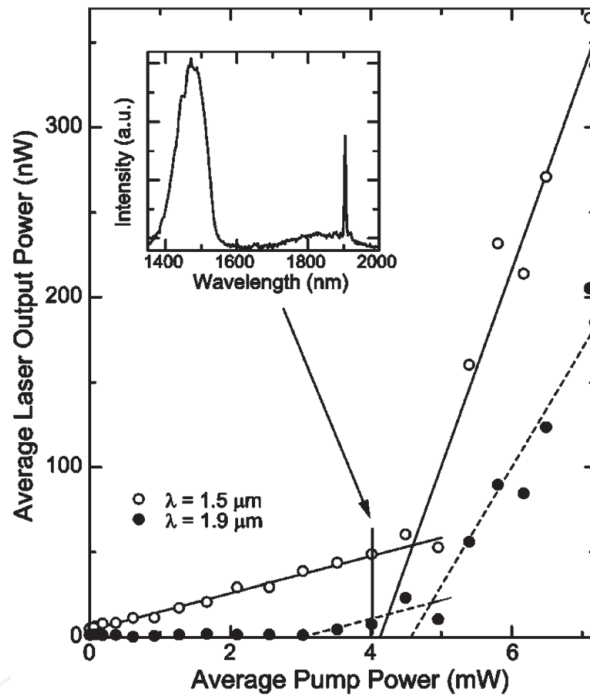


**Figure 30.** Average laser output power against average pump power for a  $Tm^{3+}$ -doped tellurite microsphere laser. (Inset) Laser emission spectrum at average pump power of  $4.0 mW$  [101].

glass. The  $Tm^{3+}$  ions are excited from  $^3F_4$  to the  $^3H_4$  energy level by the 802 nm pump laser, and the lifetime of  $Tm^{3+}$ -doped and  $Tm^{3+}$ - $Ho^{3+}$  co-doped material are shown in **Figure 32**. The emission process originates from the  $Tm^{3+}: ^3H_4 \rightarrow ^3F_4$  transition, and the energy transfer efficiency of the  $Tm^{3+}: ^3F_4$  level to  $Ho^{3+}: ^5I_7$  level is 34.9% in  $Tm^{3+}$ - $Ho^{3+}$  co-doped tellurite glass sample.

### 3.3 Summary

The last two decades have witnessed significant progress of tellurite fiber-based SC light sources, whose original progress was primarily implemented through the development of microstructured and all-solid fiber devices. The microstructured fiber demonstrated greater flexibility in tailoring the dispersion profile than the



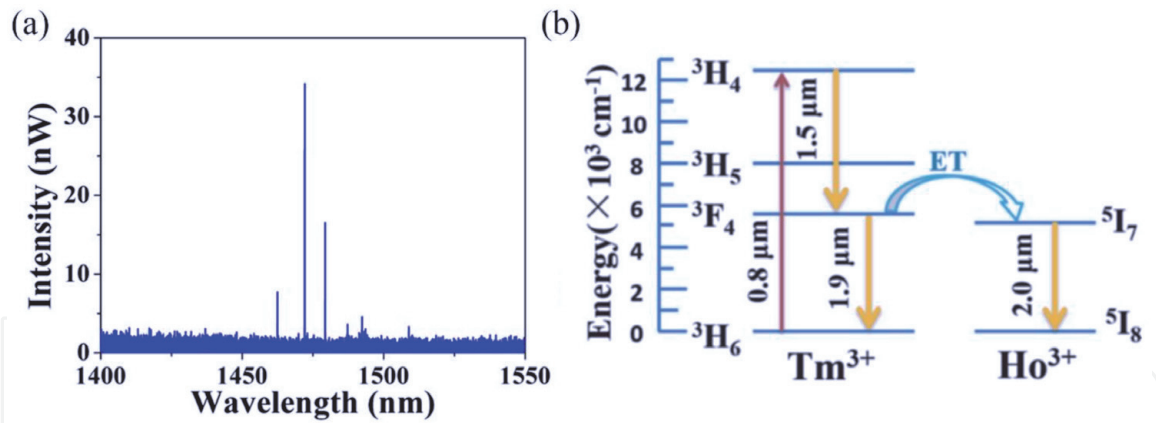


**Figure 31.** (a) Laser emission spectrum from the  $\text{Tm}^{3+}$ - $\text{Ho}^{3+}$  co-doped microsphere when the pump power was set to 2.5 mW. (b) Energy level diagram and energy transfer model in tellurite glass [3].

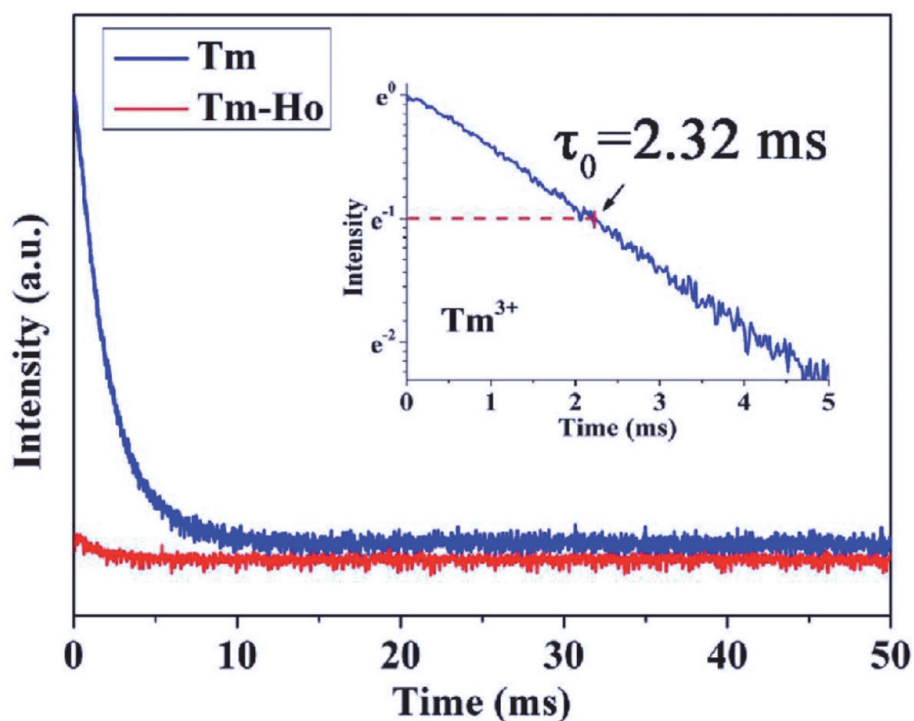


**Figure 32.** Fluorescence decay curves of  $\text{Tm}^{3+}$ - $\text{Ho}^{3+}$  co-doped and  $\text{Tm}^{3+}$ -doped tellurite glass samples at 1.9  $\mu\text{m}$ . The inset figure shows that the lifetime of  $\text{Tm}^{3+}$  at 1.9  $\mu\text{m}$  is 2.32 ms in  $\text{Tm}^{3+}$ -doped tellurite glass samples [3].

all-solid version, which provided greater options for using different pump sources, producing higher coherence. In the case of high-power output and stable MIR SC generation, the all-solid tellurite fiber performed much better than the microstructured one, and hence the fluorotellurite fiber is a promising candidate for high-power Mid-IR laser emission. Potentially this technology could be expected to reach the hundred-watt output level even after losses with careful design for heat management, fiber structure, and pump parameter optimization.

Tellurite glass microsphere resonators have overcome the limitations associated with traditional resonators in terms of glass materials. In the future, it is envisaged that tellurite glass microsphere resonators will have wide-ranging applications in photonics, having a high Q value and fast response. Meanwhile, doping rare earth ions in different host materials is expected to achieve higher-power output and more efficient lasers accessing different wavelength ranges, most notably in the infrared band.

IntechOpen

### Author details

Pengfei Wang<sup>1,2\*</sup>, Shijie Jia<sup>1</sup>, Xiaosong Lu<sup>1</sup>, Yuxuan Jiang<sup>1</sup>, Jibo Yu<sup>1</sup>, Xin Wang<sup>1</sup>, Shunbin Wang<sup>1</sup> and Elfed Lewis<sup>3</sup>

1 Key Laboratory of In-Fiber Integrated Optics of Ministry of Education, College of Physics and Optoelectronic Engineering, Harbin Engineering University, Harbin, China

2 Key Laboratory of Optoelectronic Devices and Systems of Ministry of Education and Guangdong Province, College of Optoelectronic Engineering, Shenzhen University, Shenzhen, China

3 Department of Electronic and Computer Engineering, Optical Fibre Sensors Research Centre, University of Limerick, Limerick, Ireland

\*Address all correspondence to: pengfei.wang@tudublin.ie

### IntechOpen

© 2020 The Author(s). Licensee IntechOpen. This chapter is distributed under the terms of the Creative Commons Attribution License (<http://creativecommons.org/licenses/by/3.0>), which permits unrestricted use, distribution, and reproduction in any medium, provided the original work is properly cited. 

## References

- [1] Stanworth JE. Tellurite glasses. *Nature*. 1952;**169**:581-582
- [2] Xing Z, Liu X, Gao S, Zhang Y, Liao M.  $\sim 3 \mu\text{m}$  fluorescence behavior of  $\text{Ho}^{3+}$  doped transparent tellurite glass ceramics. *Journal of Luminescence*. 2019;**215**:116562
- [3] Li A, Li W, Zhang M, Zhang Y, Wang S, Yang A, et al.  $\text{Tm}^{3+}$ - $\text{Ho}^{3+}$  codoped tellurite glass microsphere laser in the  $1.47 \mu\text{m}$  wavelength region. *Optics Letters*. 2019;**44**:511-513
- [4] Li A, Dong Y, Wang S, Jia S, Brambilla G, Wang P. Infrared-laser and upconversion luminescence in  $\text{Ho}^{3+}$ - $\text{Yb}^{3+}$  codoped tellurite glass microsphere. *Journal of Luminescence*. 2020;**218**:116826
- [5] Berzelius J. Tellurite glasses. *Annal. Physike Chemie*. 1834;**32**:577
- [6] Lambson E, Saunders G, Bridge B, El-Mallawany R. The elastic behaviour of  $\text{TeO}_2$  glass under uniaxial and hydrostatic pressure. *Journal of Non-Crystalline Solids*. 1984;**69**:117-133
- [7] El-Mallawany R. The optical properties of tellurite glasses. *Journal of Applied Physics*. 1992;**72**:1774-1777
- [8] Westman A, Crowther J. Constitution of soluble phosphate glasses. *Journal of the American Ceramic Society*. 1954;**37**:420-427
- [9] El-Mallawany R. Tellurite glasses part 1. Elastic properties. *Materials Chemistry & Physics*. 1998;**53**:93-120
- [10] El-Mallawany R. Structural and vibrational investigations of thermal properties of tellurite glasses. *Journal of Materials Research*. 1992;**7**:224-228
- [11] Liu J, Xiao Y, Huang S, Mao L, Wang W, Zhang Q. The glass-forming region and  $2.7 \mu\text{m}$  emission of  $\text{Er}^{3+}$ -doped  $\text{TeO}_2$ - $\text{Ta}_2\text{O}_5$ - $\text{ZnO}$  tellurite glass. *Journal of Non-Crystalline Solids*. 2019;**522**:119564
- [12] Wang J, Vogel E, Snitzer E. Tellurite glass: A new candidate for fiber devices. *Optical Materials*. 1994;**3**:187-203
- [13] Mori A, Ohishi Y, Sudo S. Erbium-doped tellurite glass fibre laser and amplifier. *Electronics Letters*. 1997;**33**:863-864
- [14] El-Mallawany RA. *Tellurite Glasses Handbook: Physical Properties and Data*. Boca Raton, Florida, USA: Taylor & Francis; 2011
- [15] Yakhkind A. Tellurite glasses. *Journal of the American Ceramic Society*. 1966;**49**:670-675
- [16] Jha A, Richards B, Jose G, Teddy-Fernandez T, Joshi P, Jiang X, et al. Rare-earth ion doped  $\text{TeO}_2$  and  $\text{GeO}_2$  glasses as laser materials. *Progress in Materials Science*. 2012;**57**:1426-1491
- [17] Vetrone F, Boyer J-C, Capobianco JA, Speghini A, Bettinelli M. 980 nm excited upconversion in an Er-doped  $\text{ZnO}$ - $\text{TeO}_2$  glass. *Applied Physics Letters*. 2002;**80**:1752-1754
- [18] Weber MJ, Myers JD, Blackburn DH. Optical properties of  $\text{Nd}^{3+}$  in tellurite and phosphotellurite glasses. *Journal of Applied Physics*. 1981;**52**:2944-2949
- [19] Manikandan N, Ryasnyanskiy A, Toulouse J. Thermal and optical properties of  $\text{TeO}_2$ - $\text{ZnO}$ - $\text{BaO}$  glasses. *Journal of Non-Crystalline Solids*. 2012;**358**:947-951
- [20] Froidevaux P, Lemièrè A, Kibler B, Désévéday F, Mathey P, Gadret G, et al. *Specialty Optical Fibers*.

Zurich, Switzerland: Optical Society of America; 2018. p. SoTh3H. 4

[21] Yong D, Shibin J, Bor-Chyuan H. Spectral properties of erbium-doped lead haloellurite glasses for 1.5  $\mu\text{m}$  broadband amplification. *Optical Materials*. 2000;**15**:123

[22] Savelii I. Fibres optiques à coeur suspendu en verre d'oxyde de tellure et génération d'effets non linéaires dans l'infrarouge au-delà de 2 microns. Autre. Université de Bourgogne; 2012 [Français]

[23] Lei Y, Ren F, Mei Y, Gao C, Zhu L, Lu A. Judd-Ofelt analysis and improvement in thermal stability and optical properties of  $\text{Er}^{3+}$  doped  $\text{TeO}_2\text{-ZnO-Na}_2\text{O-B}_2\text{O}_3\text{-GeO}_2$  glasses. *Materials Research Innovations*. 2014; **18**:259-266

[24] Moiseev A, Dorofeev V, Chilyasov A, Kraev I, Churbanov M, Kotereva T, et al. Production and properties of high purity  $\text{TeO}_2\text{-ZnO-Na}_2\text{O-Bi}_2\text{O}_3$  and  $\text{TeO}_2\text{-WO}_3\text{-La}_2\text{O}_3\text{-MoO}_3$  glasses. *Optical Materials*. 2011;**33**:1858-1861

[25] Lakshminarayana G, Qiu J, Brik M, Kumar G, Kityk I. Spectral analysis of  $\text{Er}^{3+}$ -,  $\text{Er}^{3+}/\text{Yb}^{3+}$ - and  $\text{Er}^{3+}/\text{Tm}^{3+}/\text{Yb}^{3+}$ -doped  $\text{TeO}_2\text{-ZnO-WO}_3\text{-TiO}_2\text{-Na}_2\text{O}$  glasses. *Journal of Physics: Condensed Matter*. 2008;**20**:375101

[26] Mazurier F, Levy M, Souquet J. Reversible and irreversible electrical switching in  $\text{TeO}_2\text{-V}_2\text{O}_5$  based glasses. *Le Journal de Physique IV*. 1992;**2**: C2-185-C182-188

[27] Dai S, Wu J, Zhang J, Wang G, Jiang Z. The spectroscopic properties of  $\text{Er}^{3+}$ -doped  $\text{TeO}_2\text{-Nb}_2\text{O}_5$  glasses with high mechanical strength performance. *Spectrochimica Acta Part A: Molecular Biomolecular Spectroscopy*. 2005;**62**: 431-437

[28] Kashchieva E, Pankova M, Dimitriev Y. Liquid phase separation in

the systems  $\text{TeO}_2\text{-B}_2\text{O}_3\text{-M}_2\text{O}_3$  ( $\text{M}_2\text{O}_3 = \text{Al}_2\text{O}_3, \text{Ga}_2\text{O}_3, \text{Sc}_2\text{O}_3, \text{La}_2\text{O}_3, \text{Bi}_2\text{O}_3$ ). *Ceramics-Silikáty*. 2001;**45**:111-114

[29] Kamalaker V, Upender G, Ramesh C, Mouli VC. Raman spectroscopy, thermal and optical properties of  $\text{TeO}_2\text{-ZnO-Nb}_2\text{O}_5\text{-Nd}_2\text{O}_3$  glasses. *Spectrochimica Acta Part A: Molecular Biomolecular Spectroscopy*. 2012;**89**: 149-154

[30] Shen S, Naftaly M, Jha A. Tungsten-tellurite—A host glass for broadband EDFA. *Optics Communications*. 2002; **205**:101-105

[31] Dimitriev Y, Dimitrov V, Arnaudov M. IR spectra and structures of tellurite glasses. *Journal of Materials Science*. 1983;**18**:1353-1358

[32] Sakida S, Hayakawa S, Yoko T. Part 2.  $^{125}\text{Te}$ NMR study of  $\text{M}_2\text{O-TeO}_2$  ( $\text{M} = \text{Li, Na, K, Rb and Cs}$ ) glasses. *Journal of Non-Crystalline Solids*. 1999;**243**:1-12

[33] Sennaroglu A, Kabalci I, Kurt A, Demirbas U, Ozen G. Spectroscopic properties of  $\text{Tm}^{3+}$ :  $\text{TeO}_2\text{-PbF}_2$  glasses. *Journal of Luminescence*. 2006;**116**:79-86

[34] Zhou D, Wang R, Yang Z, Song Z, Yin Z, Qiu J. Spectroscopic properties of  $\text{Tm}^{3+}$  doped  $\text{TeO}_2\text{-R}_2\text{O-L}_2\text{O}_3$  glasses for 1.47  $\mu\text{m}$  optical amplifiers. *Journal of Non-Crystalline Solids*. 2011;**357**: 2409-2412

[35] Elkhoshkhany N, Abbas R, El-Mallawany R, Fraih A. Optical properties of quaternary  $\text{TeO}_2\text{-ZnO-Nb}_2\text{O}_5\text{-Gd}_2\text{O}_3$  glasses. *Ceramics International*. 2014;**40**:14477-14481

[36] Neov S, Kozhukharov V, Gerasimova I, Krezhov K, Sidzhimov B. A model for structural recombination in tellurite glasses. *Journal of Physics C: Solid State Physics*. 1979;**12**:2475

[37] Jha A, Richards BDO, Jose G, Toney Fernandez T, Hill CJ, Lousteau J, et al.



Review on structural, thermal, optical and spectroscopic properties of tellurium oxide based glasses for fibre optic and waveguide applications. *International Materials Reviews*. 2012; **57**:357-382

[38] Tatsumisago M, Lee S-K, Minami T, Kowada Y. Raman spectra of TeO<sub>2</sub>-based glasses and glassy liquids: Local structure change with temperature in relation to fragility of liquid. *Journal of Non-Crystalline Solids*. 1994;**177**:0-163

[39] Sekiya T, Mochida N, Ohtsuka A, Tonokawa M. Normal vibrations of two polymorphic forms of TeO<sub>2</sub> crystals and assignments of Raman peaks of pure TeO<sub>2</sub> glass. *Journal of the Ceramic Society of Japan*. 1989;**97**:1435-1440

[40] Zhou B, Rapp CF, Driver JK, Myers MJ, Myers JD, Goldstein J, et al. *Oxide-based Materials and Devices IV*. Vol. 8626. San Francisco, California, USA: International Society for Optics and Photonics; 2013. p. 86261F

[41] Kaur A, Khanna A, Sathe VG, Gonzalez F, Ortiz B. Optical, thermal, and structural properties of Nb<sub>2</sub>O<sub>5</sub>-TeO<sub>2</sub> and WO<sub>3</sub>-TeO<sub>2</sub> glasses. *Phase Transitions*. 2013;**86**:598-619

[42] Souri D, Salehizadeh SA. Glass transition, fragility, and structural features of amorphous nickel-tellurate-vanadate samples. *Journal of Thermal Analysis Calorimetry*. 2013;**112**:689-695

[43] Aida K, Komatsu T, Dimitrov V. Thermal stability, electronic polarisability and optical basicity of ternary tellurite glasses. *Physics Chemistry of Glasses*. 2001;**42**:103-111

[44] Ohishi Y. *Optical Components and Materials IV*. Vol. 6469. International Society for Optics and Photonics; 2007. p. 646908

[45] Mohamed E, Ahmad F, Aly K. Effect of lithium addition on thermal

and optical properties of zinc-tellurite glass. *Journal of Alloys & Compounds*. 2012;**538**:230-236

[46] Maiman TH. *The Laser Inventor: Memoirs of Theodore H. Maiman*. Cham: Springer International Publishing; 2018. pp. 279-280

[47] Javan A, Bennett WR, Herriott DR. Population inversion and continuous optical maser oscillation in a gas discharge containing a He-Ne mixture. *Physical Review Letters*. 1961;**6**:106-110

[48] Hall RN, Fenner GE, Kingsley JD, Soltys TJ, Carlson RO. Coherent light emission from GaAs junctions. *Physical Review Letters*. 1962;**9**:366-368

[49] Koester CJ, Snitzer E. Amplification in a fiber laser. *Applied Optics*. 1964;**3**: 1182-1186

[50] Kao KC, Hockham GA. In: Brown J, editor. *Electromagnetic Wave Theory*. Pergamon; 1967. pp. 441-444

[51] Kawanishi S, Takara H, Uchiyama K, Shake I, Mori K. 3 Tbit/s (160 Gbit/s×19 ch) OTDM/WDM transmission experiment. In: *Optical Fiber Communication Conference (OFC)*; San Diego, California United States. 1999

[52] Yao C, Jia Z, Li Z, Jia S, Zhao Z, Zhang L, et al. High-power mid-infrared supercontinuum laser source using fluorotellurite fiber. *Optica*. 2018;**5**: 1264-1270

[53] Feng X, Shi J, Segura M, White NM, Kannan P, Loh WH, et al. Halo-tellurite glass fiber with low OH content for 2-5µm mid-infrared nonlinear applications. *Optics Express*. 2013;**21**: 18949

[54] Savelii I, Desevedavy F, Jules J-C, Gadret G, Fatome J, Kibler B, et al. Management of OH absorption in tellurite optical fibers and related supercontinuum generation. *Optical Materials*. 2013;**35**:1595-1599



- [55] Ebendorff-Heidepriem H, Kuan K, Oermann MR, Knight K, Monro TM. Extruded tellurite glass and fibers with low OH content for mid-infrared applications. *Optical Materials Express*. 2012;**2**:432
- [56] Wei C, Zhu X, Norwood RA, Song F, Peyghambarian N. Numerical investigation on high power mid-infrared supercontinuum fiber lasers pumped at 3  $\mu\text{m}$ . *Optics Express*. 2013;**21**:29488
- [57] Ohishi Y, Mori A, Yamada M, Ono H, Nishida Y, Oikawa K. Gain characteristics of tellurite-based erbium-doped fiber amplifiers for 1.5- $\mu\text{m}$  broadband amplification. *Optics Letters*. 1998;**23**:274-276
- [58] Dong J, Wei YQ, Wonfor A, Penty RV, White IH, Lousteau J, et al. Dual-pumped tellurite fiber amplifier and tunable laser using Er/Ce codoping scheme. *IEEE Photonics Technology Letters*. 2011;**23**:736-738
- [59] Oermann MR, Ebendorff-Heidepriem H, Ottaway DJ, Lancaster DG, Monro TM. Extruded microstructured fiber lasers. *IEEE Photonics Technology Letters*. 2012;**24**:578-580
- [60] Chillcce EF, Narro-García R, Menezes JW, Rodriguez E, Marconi JD, Fragnito HL, et al. National Fiber Optic Engineers Conference. Los Angeles, California: Optical Society of America; 2012. p. JW2A.27
- [61] Chuan-fei Y, Zhi-xu J, Shun-bin W.  $\text{Tm}^{3+}$  doped tellurite microstructure fiber laser. *Chinese Journal of Luminescence*. 2014;**35**:1109-1113
- [62] Xiang-wei M, Chuan-fei Y, Shan-de W.  $\text{Tm}^{3+}/\text{Ho}^{3+}$  co-doped tellurite microstructure fiber lasers. *Chinese Journal of Luminescence*. 2015;**36**:94-98
- [63] Alfano RR. *The Supercontinuum Laser Source: The Ultimate White Light*. Springer; 2016
- [64] Alfano RR, Shapiro SL. Emission in the region 4000 to 7000  $\text{\AA}$  via four-photon coupling in glass. *Physical Review Letters*. 1970;**24**:584-587
- [65] Alfano RR, Shapiro SL. Observation of self-phase modulation and small scale filaments in crystals and glasses. *Physical Review Letters*. 1970;**24**:592-594
- [66] Alfano RR, Shapiro SL. Picosecond spectroscopy using the inverse Raman effect. *Chemical Physics Letters*. 1971;**8**:631-633
- [67] Dudley JM, Genty G, Coen S. Supercontinuum generation in photonic crystal fiber. *Reviews of Modern Physics*. 2006;**78**:1135-1184
- [68] Dudley JM, Taylor JR. Cambridge CB2 1TN, UK: Cambridge University Press; 2010
- [69] Huang D, Swanson EA, Lin CP, Schuman JS, Stinson WG, Chang W, et al. Optical coherence tomography. *Science*. 1991;**254**:1178
- [70] Hartl I, Li XD, Chudoba C, Ghanta RK, Ko TH, Fujimoto JG, et al. Ultrahigh-resolution optical coherence tomography using continuum generation in an air-silica microstructure optical fiber. *Optics Letters*. 2001;**26**:608-610
- [71] Brown DM, Shi K, Liu Z, Philbrick CR. Long-path supercontinuum absorption spectroscopy for measurement of atmospheric constituents. *Optics Express*. 2008;**16**:8457-8471
- [72] Kumar VVRK, George AK, Knight JC, Russell PSJ. Tellurite photonic crystal fiber. *Optics Express*. 2003;**11**:2641-2645

- [73] Domachuk P, Wolchover NA, Cronin-Golomb M, Wang A, George AK, Cordeiro CMB, et al. Over 4000 nm bandwidth of mid-IR supercontinuum generation in sub-centimeter segments of highly nonlinear tellurite PCFs. *Optics Express*. 2008;**16**:7161-7168
- [74] Feng X, Loh WH, Flanagan JC, Camerlingo A, Dasgupta S, Petropoulos P, et al. Single-mode tellurite glass holey fiber with extremely large mode area for infrared nonlinear applications. *Optics Express*. 2008;**16**:13651-13656
- [75] Liao M, Chaudhari C, Qin G, Yan X, Suzuki T, Ohishi Y. Tellurite microstructure fibers with small hexagonal core for supercontinuum generation. *Optics Express*. 2009;**17**:12174-12182
- [76] Qin G, Yan X, Kito C, Liao M, Suzuki T, Mori A, et al. Highly nonlinear tellurite microstructured fibers for broadband wavelength conversion and flattened supercontinuum generation. *Journal of Applied Physics*. 2010;**107**:043108
- [77] Savelli I, Mouawad O, Fatome J, Kibler B, Désévéday F, Gadret G, et al. Mid-infrared 2000-nm bandwidth supercontinuum generation in suspended-core microstructured. *Optics Express*. 2012;**20**:27083-27093
- [78] Belal M, Xu L, Horak P, Shen L, Feng X, Ettabib M, et al. Sulfide and tellurite optical fibers. *Optics Letters*. 2015;**40**:2237-2240
- [79] Klimczak M, Stepniewski G, Bookey H, Szolno A, Stepien R, Pysz D, et al. Mid-infrared supercontinuum generation in suspended core tellurite microstructured optical fibers. *Optics Letters*. 2013;**38**:4679-4682
- [80] Yao C, He C, Jia Z, Wang S, Qin G, Ohishi Y, et al. Holmium-doped fluorotellurite microstructured fibers for 2.1  $\mu\text{m}$  lasing. *Optics Letters*. 2015;**40**:4695-4698
- [81] Wang F, Wang K, Yao C, Jia Z, Wang S, Wu C, et al. Tapered fluorotellurite microstructured fibers for broadband supercontinuum generation. *Optics Letters*. 2016;**41**:634-637
- [82] Price JHV, Feng X, Heidt AM, Brambilla G, Horak P, Poletti F, et al. Supercontinuum generation in non-silica fibers. *Optical Fiber Technology*. 2012;**18**:327-344
- [83] Thapa R, Rhonehouse D, Nguyen D, Wiersma K, Smith C, Zong J, et al. *SPIE*. 2013;**8898**:889808:1-8
- [84] Kedenburg S, Steinle T, Mörz F, Steinmann A, Nguyen D, Rhonehouse D, et al. Solitonic supercontinuum of femtosecond mid-IR pulses in W-type index tellurite fibers with two zero dispersion wavelengths. *APL Photonics*. 2016;**1**:086101
- [85] Kedenburg S, Strutynski C, Kibler B, Froidevaux P, Désévéday F, Gadret G, et al. High repetition rate mid-infrared supercontinuum generation from 1.3 to 5.3  $\mu\text{m}$  in robust step-index tellurite fibers. *Journal of the Optical Society of America B*. 2017;**34**:601-607
- [86] Shi H, Feng X, Tan F, Wang P, Wang P. Multi-watt mid-infrared supercontinuum generated from a dehydrated large-core tellurite glass fiber. *Optical Materials Express*. 2016;**6**:3967-3976
- [87] Jia Z, Yao C, Jia S, Wang F, Wang S, Zhao Z, et al. 4.5 W supercontinuum generation from 1017 to 3438 nm in an all-solid fluorotellurite fiber. *Applied Physics Letters*. 2017;**110**:261106
- [88] Jia ZX, Yao CF, Jia SJ, Wang F, Wang SB, Zhao ZP, et al. Supercontinuum generation covering

the entire 0.4–5  $\mu\text{m}$  transmission window in a tapered ultra-high numerical aperture all-solid fluorotellurite fiber. *Laser Physics Letters*. 2018;**15**:025102

[89] Zou C-L, Shu F-J, Sun F-W, Gong Z-J, Han Z-F, Guo G-C. Theory of free space coupling to high-Q whispering gallery modes. *Optics Express*. 2013;**21**:9982-9995

[90] Little BE, Laine J-P, Haus HA. Analytic theory of coupling from tapered fibers and half-blocks into microsphere resonators. *Journal of Lightwave Technology*. 1999;**17**:704

[91] Murphy RM, Lei F, Ward JM, Yang Y, Chormaic SN. Bandpass transmission spectra of a whispering gallery microcavity coupled to an ultrathin fiber. *Optics Express*. 2017;**25**:13101-13106

[92] Yu J, Lewis E, Farrell G, Wang P. Compound glass microsphere resonator devices. *Micromachines*. 2018;**9**:356

[93] Yang Z, Wu Y, Zhang X, Zhang W, Xu P, Dai S. Low temperature fabrication of chalcogenide microsphere resonators for thermal sensing. *IEEE Photonics Technology Letters*. 2016;**29**:66-69

[94] Yang Z, Wu Y, Yang K, Xu P, Zhang W, Dai S, et al. Fabrication and characterization of  $\text{Tm}^{3+}$ - $\text{Ho}^{3+}$  co-doped tellurite glass microsphere lasers operating at  $\sim 2.1 \mu\text{m}$ . *Optical Materials*. 2017;**72**:524-528

[95] Yu J, Lewis E, Brambilla G, Wang P. Temperature sensing performance of microsphere resonators. *Sensors*. 2018;**18**:2515

[96] Sasagawa K, Kusawake K, Ohta J, Nunoshita M. Nd-doped tellurite glass microsphere laser. *Electronics Letters*. 2002;**38**:1355-1357

[97] Peng X, Song F, Gonokami MK, Jiang S, Peyghambarian NN.  $\text{Er}^{3+}$ -doped tellurite glass microsphere laser: Optical properties, coupling scheme, and lasing characteristics. *Optical Engineering*. 2005;**44**:034202

[98] Zhao H, Yi Y, Wang X, Li A, Yang A, Yang Z, et al. Triple-wavelength lasing at 1.50  $\mu\text{m}$ , 1.84  $\mu\text{m}$  and 2.08  $\mu\text{m}$  in a  $\text{Ho}^{3+}/\text{Tm}^{3+}$  co-doped fluorozirconate glass microsphere. *Journal of Luminescence*. 2019:116889

[99] Wu J, Jiang S, Qiu T, Morrell M, Schulzgen A, Peyghambarian N. *Optical Components and Materials II*. Vol. 38. International Society for Optics and Photonics; 2015. pp. 1355-1357

[100] Percival R, Szebesta D, Williams J, Lauder R, Tropper A, Hanna D. Diode pumped operation of thulium doped fluoride fibre amplifier suitable for first window systems. *Electronics Letters*. 1994;**30**:1598-1599

[101] Sasagawa K, Yonezawa Z-O, Iwai R, Ohta J, Nunoshita M. S-band  $\text{Tm}^{3+}$ -doped tellurite glass microsphere laser via a cascade process. *Applied Physics Letters*. 2004;**85**:4325-4327